THESIS FOR THE DEGREE OF DOCTOR OF PHILOSOPHY

Key Signal Processing Technologies for High-speed Passive Optical Networks

Lei Xue

CHALMERS
UNIVERSITY OF TECHNOLOGY

Optical Networks Group
Department of Electrical Engineering
Chalmers University of Technology
Göteborg, Sweden 2021

Key Signal Processing Technologies for High-speed Passive Optical Networks

Lei Xue

ISBN 978-91-7905-577-6

Doktorsavhandlingar vid Chalmers Tekniska Högskola
Ny serie 5044
ISSN 0346-718X

Department of Electrical Engineering
Chalmers University of Technology
SE-412 96 Göteborg, Sweden
Phone: +46 (0)31 772 1000
www.chalmers.se

Typeset by the author using LaTeX.

Printed by Chalmers Reproservice
Göteborg, Sweden 2021

To my parents.

Abstract

With emerging technologies such as high-definition video, virtual reality, and cloud computing, bandwidth demand in the access networks is ever-increasing. Passive optical network (PON) has become the promising architecture thanks to its low cost and easy management. IEEE and ITU-T standard organizations have been standardizing the next-generation PON, targeting on increasing the single-channel capacity from 10 Gb/s to 25, 50, and 100 Gb/s as the solution to address the dramatic increase of bandwidth demand. However, since the access network is extremely cost-sensitive, many research problems imposed in the physical layer of PON need to be addressed in a cost-efficient way, which is the primary focus of this thesis.

Utilizing the low-cost 10G optics to build up high-speed PON systems is a promising approach, where signal processing techniques are key of importance. Two categories of signal processing techniques have been extensively investigated, namely optical signal processing (OSP) and digital signal processing (DSP). Dispersion-supported equalization (DSE) as a novel OSP scheme is proposed to achieve bit-rate enhancement from 10 Gb/s to 25 Gb/s based on the 10G-class optics. Thanks to the bandwidth improved by DSE, the non-return-zero on-off keying, which is the simplest modulation format, is able to be adopted in the PON system without complex modulation or DSP. Meanwhile, OSP is also proposed to work together with DSP enabling 50G PON while simplifying the DSP complexity. Using both DSE and simple feed-forward equalizer is able to support 50 Gb/s PAM-4 transmission with 10G optics. For C-band 50 Gb/s transmission, injection locking techniques as another OSP approach is proposed to compress the directly modulated laser chirp and increase system bandwidth in the optical domain where a doubled capacity from 25 Gb/s to 50 Gb/s over 20 km fiber can be built on top of 10G optics. For DSP, we investigate the advantages of neural network (NN) on the mitigation of the time-varying nonlinear semiconductor optical amplifier pattern effect. In order to reduce the expense caused by the high computation complexity of NN, a pre- equalizer is introduced at the central office that allows cost-sharing for all connected access users. In order to push the PON system line rate to 100 Gb/s, a joint nonlinear Tomlinson-Harashima precoding-Volterra algorithm is proposed to compensate for both linear and nonlinear distortions where 100 Gb/s PAM-4 transmission over 20 km fiber with 15 GHz system bandwidth can be achieved.

Keywords: Optical access network, passive optical network, optical signal processing, digital signal processing, dispersion supported equalization, semiconductor optical amplifier, neural network.

List of papers

This thesis is based on the following publications:

[A] **L. Xue**, L. Yi, H. Ji, P. Li, and W. Hu, "First demonstration of symmetric 100G-PON in O-band with 10G-class optical devices enabled by dispersion-supported equalization". *Optical Fiber Communication Conference and Exhibition (OFC)*, paper M3H.1, Los Angeles, USA, 2017.

[B] **L. Xue**, L. Yi, H. Ji, P. Li, and W. Hu, "Symmetric 100-Gb/s TWDM-PON based on 10G-class optical devices enabled by dispersion-supported equalization". *Journal of Lightwave Technology*, vol. 36, no. 2, pp. 580–586, 2018.

[C] **L. Xue**, L. Yi, H. Ji, Z. Li, and W. Hu, "First real-time demonstration of symmetric 100G-PON". *Asia Communications and Photonics Conference and Exhibition (ACP)*, paper AS4A.3, Wuhan, China, 2016.

[D] **L. Xue**, R. Lin, J. V. Kerrebrouck, L. Yi, J. Chen, and X. Yin, "100G PAM-4 PON with 34 dB power budget using joint nonlinear Tomlinson-Harashima precoding and Volterra equalization". *European Conference and Exhibition on Optical Communication (ECOC)*, paper We4F.5, Bordeaux, France, 2021.

[E] **L. Xue**, L. Yi, R. Lin, L. Huang, and J. Chen, "SOA pattern effect mitigation by neural network-based pre-equalizer for 50G PON". *Optics Express*, vol. 16, no. 16, pp. 24714-24722, 2021.

[F] **L. Xue**, L. Yi, P. Li, and W. Hu, "50-Gb/s TDM-PON based on 10G-class devices by optics-simplified DSP". *Optical Fiber Communication Conference and Exhibition (OFC)*, paper M2B.4, San Diego, USA, 2018.

[G] **L. Xue**, L. Yi, W. Hu, R. Lin, and J. Chen, "Optics-simplified DSP for 50 Gb/s PON downstream transmission using 10 Gb/s optical devices". *Journal of Lightwave Technology*, vol. 38, no. 3, pp. 583-589, 2020.

[H] **L. Xue**, L. Yi, L. Zhang, O. Ozolins, A. Udalcovs, X. Pang, and J. Chen, "50-Gb/s dispersion-unmanaged DMT transmission with injection locked 10G-class 1.55-μm DML". *Conference on Lasers and Electro-Optics (CLEO)*, paper SW4O.2, San Jose, USA, 2019.

Other publications by the author, not included in this thesis, are:

[I] **L. Xue**, L. Yi, and W. Hu, "4×25-Gb/s NRZ-OOK signals transmission over 160-km single mode fiber using 10G-class DML and photodiode". *IEEE Photonics Journal*, vol. 10, no. 3, pp. 7103508, 2018.

[J] L. Huang, **L. Xue**, Q. Zhuge, W. Hu, and L. Yi, "Modulation format identification under stringent bandwidth limitation based on an artificial neural network". *OSA Continuum*, vol. 4, no. 1, pp 96-104, 2021.

[K] T. Liao, **L. Xue**, L. Huang, W. Hu, and L. Yi, "Training data generation and validation for a neural network-based equalizer". *Optics Letters*, vol. 45, no. 18, pp. 5113-5116, 2020.

[L] T. Liao, **L. Xue**, W. Hu, L. Yi, "Unsupervised learning for neural network-based blind equalization". *IEEE Photonics Technology Letters*, vol. 32, no. 10, pp. 569-572, 2020.

[M] L. Yi, **L. Xue**, and W. Hu, "Simplified signal processing for high-speed PON". *Conference on Lasers and Electro-Optics Pacific Rim (CLEO)*, paper Th4l.1, Hong Kong, China, 2018.

[N] L. Yi, **L. Xue**, H. Ji, and W. Hu, "Field demonstration of real-time 100G-PON". *SPIE Photonics West*, San Francisco, USA, 2017.

[O] L. Yi, T. Liao, L. Huang, **L. Xue**, P. Li, and W. Hu, "Machine learning for 100 gb/s/λ passive optical network". *Journal of Lightwave Technology*, vol. 37, no. 6, pp. 1621-1630, 2019.

[P] P. Li, L. Yi, **L. Xue**, and W. Hu, "56 Gbps IM/DD PON based on 10G-class optical devices with 29 dB loss budget enabled by machine learning". *Optical Fiber Communication Conference and Exhibition (OFC)*, paper M2B.2, San Diego, USA, 2018.

[Q] P. Li, L. Yi, **L. Xue**, and W. Hu, "100 Gbps IM/DD transmission over 25km SSMF using 20G-class DML and PIN enabled by machine learning". *Optical Fiber Communication Conference and Exhibition (OFC)*, paper W2A.46, San Diego, USA, 2018.

[R] H. Ji, L. Yi, Z. Li, **L. Xue**, X. Li, Q. Yang, S. Wang, Y. Yang, S. Yu, and W. Hu, "Field demonstration of a real-time 100-Gb/s PON based on 10G-class optical devices". *IEEE Journal of Lightwave Technology*, vol. 35, no. 10, pp. 1914-1921, 2017.

[S] H. Ji, L. Yi, **L. Xue**, M. Tang, Y. Fu, Z. Feng, L. Gan, W. Hu, "700G/280G SDM-TWDM-PON over 20 km seven-core fibre based on 10G-class optical components". *Asia Communications and Photonics Conference and Exhibition (ACP)*, paper AF3A.3, Wuhan, China, 2016.

Acknowledgments

I would like to express my gratitude to Prof. Jiajia Chen for being my examiner and main supervisor and for giving me the opportunity to join the Optical Networks group as a Ph.D. student. Thanks for all the guidance, nice discussions, and the constant support you have provided me for the last couple of years. This has not only helped me develop a mature scientific mindset and also a positive and professional attitude as a researcher. This deepest gratitude also goes to my co-supervisor, Dr. Rui Lin, for her valuable time reviewing all my rough papers and providing detailed comments and guidance, which have helped improve my writing skills. I would also like to express my thanks to the head of our group, Profs. Paolo Monti and Lena Wosinska, for giving me support when there is a need. I am also grateful to Prof. Xin Yin for giving me the chance to finish my experiment at iMec-Gent university.

Special thanks go to Hao Guo for reading the rough draft of my paper and all the help he has provided me outside of my research. I am also grateful to Prof. Lilin Yi, Dr. Xiaodang Pang, Dr. Lu Zhang, Dr. Jun Li, Dr. Aleksejs Udalcovs, Dr. Oskars Ozolins, and Dr. Joris Van Kerrebrouck for all the nice discussions and collaborations we have had.

I thank all my former and current colleagues at the Optical Networks group for making my time here such an unparalleled experience. Many thanks to the head of our division, Prof. Erik Ström, for ensuring a stimulating and joyful research atmosphere. Special thanks to Maryam Lashgari, Ehsan Etezadi, and Dr. Carlos Natalino Da Silva, for our excellent collaborations in the teaching work and fond memories in after-work fun. Also, many thanks go to Prof. Henk Wymeersch, Associate Prof. Marija Furdek Prekratic, and Prof. Erik Agrell for all the exciting discussions in the meeting and Fika time. I am also grateful to Natasha and Daniela for helping me with all the administrative or organizational issues. Thank you, Chao, Chenjie, Yu, Bo, Huang, Yuxuan, and Shen, for all the support and encouragement you have given to me. I would also like to thank all my Chinese friends in Gothenburg for all the great moments we have experienced together.

Finally, I'd like to express my deepest gratitude towards my sister, mom, and dad for all their constant support, love, and encouragement over the years. I love you.

Lei Xue

Göteborg
November, 2021

Financial support

This work was financially supported by the H2020 project 5G System Technological Enhancements Provided by Fiber Wireless Deployments (5G STEP FWD).

Acronyms

ADC/DAC	Analog-to-digital/digital-to-analog converter
AM	Amplitude modulation
AON	Active optical network
APD	Avalanche photodiode
AR	Augmented reality
ASIC	Application-specific integrated circuit
ATM	Asynchronous transfer mode
BtB	Back-to-back
CAGR	Compound annual growth rate
CD	Chromatic dispersion
CMOS	Complementary metal-oxide-semiconductor
CO	Central office
C-RAN	Cloud-radio access network
CWDM	Coarse wavelength-division-multiplexer
DB-PAM-4	Duobinary PAM-4
DFB	Distributed feedback laser
DFE	Decision feedback equalizer
DML	Directly modulated laser
DMT	Discrete multitone
DSF	Dispersion-shifted fiber
DSE	Dispersion-supported equalization
DSP	Digital signal processing
DSL	Digital subscriber line
DWDM	Dense wavelength division multiplexing

EAM	Electro-absorption modulated laser
EDC	Electrical dispersion compensation
EDB	Electrical duobinary
EOM	Electro-optic modulator
EPON	Ethernet passive optical network
FBG	Fiber Bragg grating
FFE	Feed forward equalizer
FFT	Fast Fourier transform
FIR	Finite impulse response
FM	Frequency modulation
FP	Fabry-Perot
FSAN	Full-service access network
FTTx	Fiber to the x
FWM	Four-wave mixing
GPON	Gigabit passive optical network
IFFT	Inverse fast Fourier transform
IMDD	Intensity modulation and direct detection
IP	Internet protocol
ISI	Individual symbol interference
LMS	Least mean square
LTHP	Linear Tomlinson-Harashima precoding
MD	Modal dispersion
MLSE	Maximum likelihood sequence estimation
ML	Master laser
MZM	Mach-Zehnder modulator
NN	Neural network

NG-PON2	Next generation PON stage 2
NRZ	Non-return to zero
NTHP	Nonlinear Tomlinson-Harashima precoding
OC	Optical circulator
ODC	Optical dispersion compensator
ODN	Optical distribution network
OFDM	Orthogonal frequency division multiplexing
OLT	Optical line terminal
ONU	Optical network unit
OOK	On-off keying
OSA	Optical spectrum analyzer
OSP	Optical signal processing
PAM-4	4-level pulse-amplitude modulation
PC	Polarization controller
PMD	Polarization mode dispersion
PON	Passive optical network
PtMP	Point-to-multipoint
PtP	Point-to-point
QAM	Quadrature amplitude modulation
RLS	Recursive least squares
SBS	Stimulated Brillouin scattering
SL	Slave laser
SMF	Single mode fiber
SNR	Signal-to-noise ratio
SOA	Semiconductor optical amplifier
SPM	Self-phase modulation

SRS	Stimulated Raman scattering
SSBI	Signal-signal beat interference
TDM	Time-division multiplexing
THP	Tomlinson-Harashima precoding
TWDM	Time and wavelength division multiplexing
UDWDM	Ultra-dense wavelength division multiplexing
VNA	Vector network analyzer
VR	Virtual reality
WDM	Wavelength division multiplexing
XPM	Cross phase modulation
XGPON	10-Gigabit passive optical network

Contents

Part I

Overview

CHAPTER 1

Introduction

The worldwide Internet traffic volume is under exceptional growth in the last 20 years, and it is expected that this trend will continue in the future. The driving force behind this trend can be attributed to the popularity of bandwidth-consuming Internet services. Therefore, a higher network capacity is needed to satisfy the tremendous growth in bandwidth requirements. The last-mile bottleneck of the Internet speed occurs in the access network. Optical fiber communication with greater bandwidth and higher capacity is gradually brought to the access network replacing the traditional copper/cable-based technologies. After years of development, the optical access network with a system capacity of 10 Gb/s is currently under deployment. Beyond 10 Gb/s optical access network is undoubtedly the next step to fulfill the bandwidth demand. With this in mind, the thesis concentrates on the next-generation high-speed optical access networks, and this chapter starts with the research background and motivation.

1.1 Background and motivation

The era of the Internet began around 1968 with the invention of the Advanced Research Projects Agency Network (ARPANET) [1], which enabled the communication of four mainframe computers located at four universities. Since then, the Internet has been evolving into a global network that connects more than 18 billion devices [2]. According to the Cisco statistics in 2020 [3], the total number of Internet users is 4.66 billion. Nearly 59.5% of the global population has access to the Internet through ei-

ther wireless or wired technology. This number is increased to 90% in North America, and 82% in Western Europe. The Internet has turned our lives upside down and it is now the prioritized medium for our everyday communication. Especially in recent years, the popularity of mobile Internet further accelerates this trend. Nowadays, we can almost do everything by simply using a smartphone. For example, ordering pizza on UberEATS, buying nearly everything on Amazon, sharing a beautiful moment with friends on Instagram, watching 4K/8K high-definition video on YouTube, and sending instant voice or video calls on WhatsApp. Virtual reality (VR) and augmented reality (AR) assisted entertainments are just around the corner.

The ever-growing number of online services are coming to the market, significantly increasing users' demand for higher bandwidth. Cisco predicts that the global Internet Protocol (IP) traffic is expected to grow at a compound annual growth rate (CAGR) of 26% from 2018 to 2023 [3]. In order to satisfy the increasing demand for online connections, the Internet is deployed on a physical network infrastructure enabling global data transfer. This network architecture adopts three hierarchical connections, namely the core network, metro network, and access network (shown in Fig. 1.1). Each layer has a different function and topology. The core network known as the backbone of the Internet uses a mesh topology providing any-to-any connections among various sub-networks. The core network links span up to several thousands of kilometers, interconnecting large cities, countries, and even continents. Then, the metro network is deployed using a ring topology providing connections between cities or metropolitan areas with a typical coverage from 40 km to a few hundreds of kilometers. Both core and metro network links are implemented with fiber-based optics, enabling Terabit communications over a large distance. Finally, access networks cover the last mile of the Internet, connecting the end users to the closest central office (CO) nodes with a few hundred meters to a few kilometers in between. Since the access network needs to connect dispersed users, a capillary-like network structure is needed to ensure enough geographic coverage. Compared to core and metro networks, access networks usually suffers from stricter cost constraints due to the limited number of customers sharing the deployment cost of the network.

The physical links in access networks nowadays are still largely relying on copper and coaxial cables, which are reaching their capacity limits. The explosive growth of global Internet traffic has made the access networks become the bottleneck in providing higher capacity. The physical infrastructure in the next generation access networks will bring optical communication closer to the user, and the optical access network is extended to cover the last mile. FTTx (where x represents a particular name or object, such as 'home' or 'building', see Fig. 1.1) is becoming a prevailing trend to keep up with the ever-growing bandwidth demand.

The global number of fixed-broadband subscriptions is 1.2 billion at the end of Q1 2021 [4]. At the same time, the share of fiber-based high-speed FTTx connections increases to 56.4%, while cable and copper-based digital subscriber line (DSL) con-

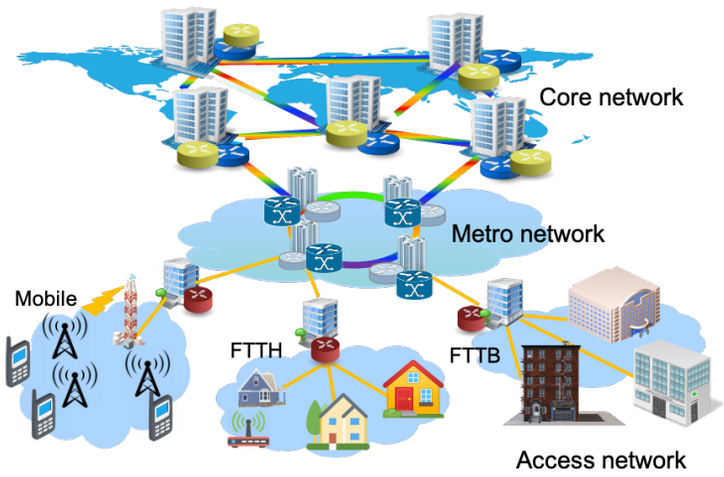

Figure 1.1: Architectures of telecommunication network. FTTH: Fiber to the home; FTTB: Fiber to the building.

nections deteriorate to 18.4% and 12.2%. At the continent level, shown in Fig. 1.2, FTTx is the dominant access technology in Asia and Oceania until Q1, 2021, whereas copper connections still have the largest market share in Africa and cable is the most popular technology in the Americas. The reason is that some developing counties in Asia, such as China and Korea, leapfrog the cable and DSL technologies, and deploy fiber infrastructure for the access networks directly. However, some counties in the Americas and Europe are trying to reuse the legacy cable and DSL equipment to avoid the large investments for new fiber implementation.

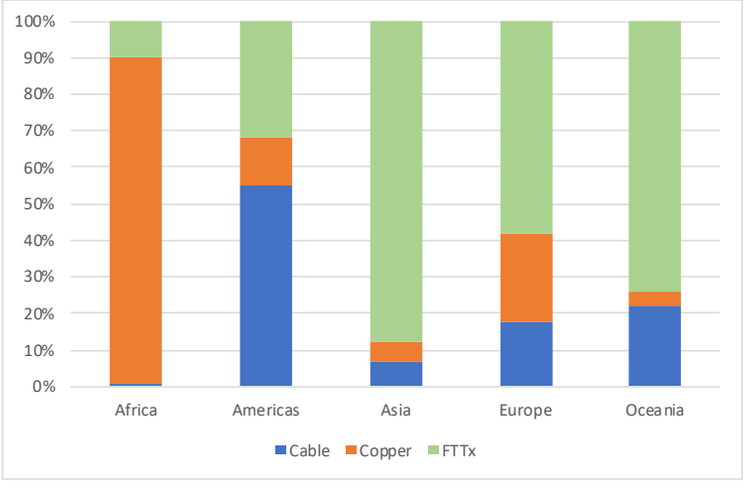

Figure 1.2: Technology market share by region in Q1, 2021 [4].

In European countries, telecommunication is managed by hundreds of different operators, making it difficult for all of them to upgrade infrastructure simultaneously. To promote the deployment of FTTH in some European countries, the European FTTH council was founded, promising to increase the access data rate to 1 Gbps per

user by 2025 [5], [6]. Every year since 2007, the Europe FTTH Council publishes a market panorama, showing the top-tier FTTH coverage in European countries. The report for 2020 is shown in Fig. 1.3. For Sweden, fiber-based fixed-broadband access coverage increases to 61.8%, absorbing the customers from all the other technologies and making fiber the dominant access medium.

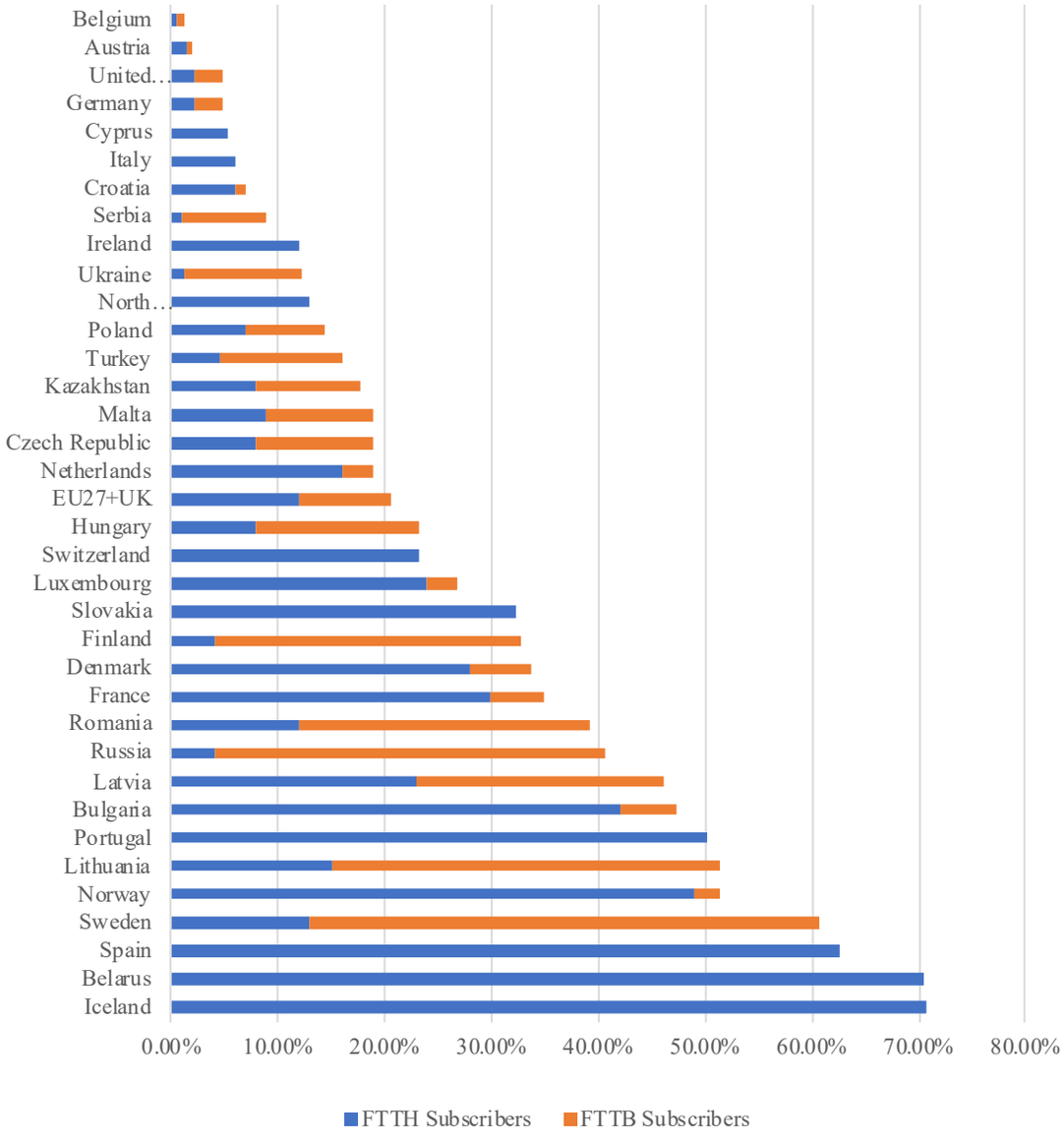

Figure 1.3: Percentage of fiber based fixed-broadband in European countries on, September 2020 [7].

Nevertheless, the sheer fiber volume required to provide a dedicated fiber connection to each customer makes it challenging to deploy FTTH. To overcome this challenge, passive optical network (PON) is proposed as a cost-effective solution for FTTH and FTTB deployment. Compared to other optical access technologies such

as active optical network (AON), the PON, with a point-to-multipoint architecture, provides a connection from the metro node to multiple users allowing partial fiber sharing and a reduction of active components in the field. After years of development, PONs are becoming the most preferred system for optical access networks. According to the latest PON market report in 2021 [8], the global PON equipment market is USD 12.6 billion in 2020, which is projected to reach USD 37.6 billion in 2027, growing at a CAGR of 16.9% from 2020 to 2027. The predicted growth is because of the increased demand for fixed broadband and the 5G mobile networks where the PON is proposed to support high-speed fronthaul links [9]–[11].

Besides increasing the number of installed PON systems, it is also important to upgrade the system capacity. Currently, the most widely deployed Gigabit-capable PON (G-PON) system with a system rate of 2.5 Gb/s in downstream and 1.25 Gb/s in upstream [12], and the following standards with either a single channel 10 Gb/s or 40 Gb/s after employing four wavelength multiplexing [13]. From 2015, the Institute of Electrical Engineers (IEEE) task force starts to standardize the next-generation Ethernet PON with a downstream speed of 100 Gb/s based on wavelength multiplexing of four 25 Gb/s channels [14]. Moreover, International Telecommunication Union (ITU) hopes to directly upgrade the data rate from single-channel 10 Gb/s to 50 Gb/s [15]. Many research institutes start to investigate the single-channel 100G PON in the downstream. To fulfill these increasing demands of higher capacity, many technical issues in the physical link need to be addressed, e.g., bandwidth limitation and nonlinear response from optoelectronics components, dispersion and power attenuation from fiber. How to increase the data rate in a cost-effective way is the research focus. A group of new signal processing technologies are required to be investigated.

1.2 Thesis overview

The research content of this thesis follows the PON evolution roadmap. Both optical and digital signal processing approaches are proposed to address the most challenging technological problems for upgrading bit rate from 10 Gb/s to 25 Gb/s, 50 Gb/s, and 100 Gb/s. Table 1.1 shows the major impairments in PON addressed in this thesis.

In order to upgrade the data rate to 25 Gb/s, the simplest solution is to employ a family of high-bandwidth optics with the non-return-zero on-off keying (NRZ-OOK) format. Nevertheless, the corresponding components' cost is too high for access networks [16]. A cost-effective solution is to reuse the legacy 10G directly modulated lasers (DMLs), available for high volume production at an affordable price [17]. Using DMLs, however, the signal quality degrades due to the bandwidth limitation and the DML chirp effect, and it gets worse after fiber transmission [18]. Similar issues occur when the transmission data rate increases up to 50 Gb/s and 100 Gb/s per wavelength. Reusing the low bandwidth DML is still the cost-effective solution by

the operators and vendors. Exploiting spectrum efficient modulation formats, such as pulse amplitude modulation 4-level (PAM-4) [19], electrical duobinary (EDB) [20], discrete multi-tone (DMT) [21], can relieve the bandwidth limitation, but these modulation formats have strict requirements on the linearity of optoelectronic components. Hence, the nonlinear impairments induced by the nonlinear response from the optics need to be addressed. From a different perspective, with the increase of data rate, the minimum optical power required at the receiver side could be higher. The high bandwidth receiver with and high sensitivity is desired to ensure enough power budget (>29 dB). Given that the commercial 25G avalanche photodiode (APD) is still costly, a semiconductor optical amplifier (SOA) combined with a larger bandwidth photodiode (PD) is a promising solution for PON [22]. However, the nonlinear pattern effect caused by SOA gain saturation degrades the signal quality at high reception power, resulting in a reduced receiving dynamic range [23]. Hence, compensation strategies must be adopted to equalize the signal from these linear and nonlinear impairments, as shown in Table 1.1.

Table 1.1: Major impairments in high-speed PON

	Major impairments	Linear/Nonlinear
Transmitter	Limited bandwidth	Linear
	Nonlinear response	Nonlinear
	Chirp	Nonlinear
Fiber	Chromatic dispersion	Linear
	Power attenuation	Linear
Receiver	Nonlinear response	Nonlinear
	Limited bandwidth	Linear
	SOA gain saturation	Nonlinear

Various compensation schemes can be employed, either optically or electrically, both at the transmitter or the receiver side. Optical signal processing (OSP) can improve the signal performance directly in the optical domain without optical-to-electrical (O/E) conversion. In **Paper A**, an OSP method named dispersion supported equalization (DSE) is proposed to increase the system bandwidth from 6 GHz to 11 GHz, enabling real-time 25 Gb/s signal transmission with 10G DML and APD. Moreover, the proposed method can support multi-channel equalization with a single component. In **Papers B** and **C**, an experimental demonstration of symmetric 4×25 Gb/s PON in both O-band and C-band based on DSE is presented, validating the effectiveness of DSE.

The bandwidth improvement from DSE is not enough for error-free transmission when the data rate increases up to 50 Gb/s. Electrical digital signal processing (DSP) can help to compensate both linear and nonlinear distortions at the bit level,

which is more flexible and powerful than the OSP. The costly high-speed analog-to-digital converter (ADC) and application-specific integrated circuit (ASIC) chip become the main obstacle for the practical deployment [24]. Putting the DSP module at the transmitter side can be a cost-effective solution since the DSP cost are shared by all users. **Paper D** proposes a joint nonlinear Tomlinson-Harashima Precoding (NTHP)-Volterra algorithm to compensate system impairments for a single-channel 100G PON. The NTHP module is implemented at the transmitter side, enabling cost-sharing among users. In **Paper E**, a neural network (NN)-based equalizer is firstly proposed to compensate the SOA pattern effect for 50G PON. Considering the high computation complexity of NN, it is used as a pre-equalizer so that the DSP cost can be shared.

In addition, the computation complexity of DSP algorithms needs further consideration for PON applications. Simplified DSP algorithms show great potentials to reduce the complexity [25], [26], which usually comes with a compromise to the performance. An alternative solution is to use OSP to improve the signal quality in the optical domain partially. In this way, the required DSP complexity can be reduced. Such a scheme is validated with experiments presented in **Papers F** and **G**. DSE is employed to improve the system bandwidth in the optical domain, and then a simple feed-forward equalizer (FFE) is used for 50 Gb/s signal transmission with 10G DML and APD. Finally, **Paper H** presents another OSP method named injection locking, which can increase the system bandwidth and compress DML chirp in the optical domain. With the help of injection locking and DSP, 50G C-band signal transmission over 20 km can be achieved.

1.3 Outline of this thesis

This thesis presents a set of signal processing technologies toward the realization of 25G, 50G, and 100G PONs. Firstly, Chapter 2 introduces the basics of optical access networks. Specifically, the types of multiplexing technologies and evolution roadmap in PON are introduced together with the discussion of modulation formats selection for the next-generation PONs. Following this, Chapter 3 is devoted to discussing major impairments in high-speed PONs, including the linear and nonlinear distortions from the optoelectronics and fiber. Also, the related impacts on the signal are introduced and discussed. In Chapter 4, OSP technologies, dispersion-supported equalization and injection locking, in particular, are introduced and discussed as solutions to address PON system impairments. Chapter 5 is mainly about DSP with the basics of the principle behind various linear and nonlinear algorithms introduced and special attention to our proposed NTHP-Volterra algorithm and NN-based pre-equalizer. Chapter 6 introduces hybrid OSP and DSP. Both DSE and injection locking are employed to reduce the complexity requirements of DSP. Chapter 7 gives an outlook of future work which is followed by a summary of appended papers in

Chapter 8.

CHAPTER 2

Passive optical networks

The communication network is developing towards all-optical networks. Optical access networks are expected to replace the copper wire access networks to meet the ever-growing bandwidth requirements. In this chapter, an overview of optical access networks is given with a focus on the PON technologies. The multiplexing technologies for high-speed transmission are introduced along with a historical review of PON standards. We also discuss the basics of the modulation formats and their potential application in the high-speed PON systems.

2.1 Optical access networks

There are several types of network topology for optical access networks, in particular point-to-point (PtP), AON, and PON, respectively (see Fig. 2.1) [27], [28]. In the PtP structure, each customer is connected to the central office (CO) through a pair of independent optical fibers, and the packet switching is performed in the CO. Although high system bandwidth can be assured in this approach, the practical deployment is expensive since there is no resource sharing leading to the fact that each user needs to cover the full cost of the corresponding link. In the AON, the packet switching is relocated from CO to a remote active node near the user side. Partial fiber sharing and reduced complexity of the switch in the central station can be achieved in this topology. Nevertheless, AONs require an additional power supply to maintain the switching operation. The active switch is replaced by a passive optical power splitter in PON. Thus, no additional power supply is required at the

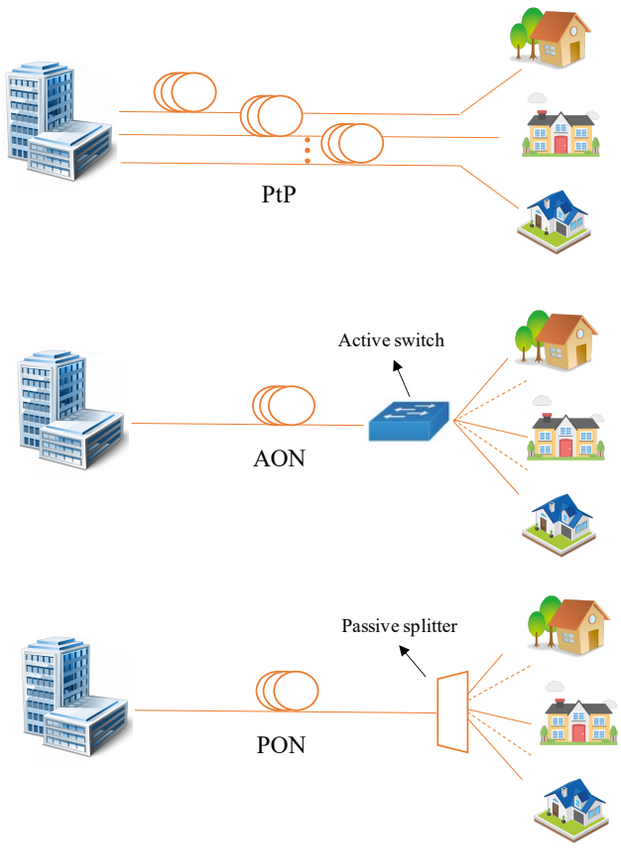

Figure 2.1: Topology of optical access networks.

remote node. A single fiber connects the CO and the user side, and when it gets close to areas with a dense number of subscribers, a passive splitter is used to connect the subscriber side over a short distance. This point-to-multipoint (PtMP) architecture enables the maximum resource sharing and the lowest installation, operation, and management costs, making PON the most well-known technology for optical access networks [29].

The architecture of PON consists of optical line terminal (OLT) located in the CO, optical network units (ONUs) on the user side, and a passive optical distribution network (ODN) connecting the OLT and ONUs as shown in Fig. 2.2. The OLT is used to control the bidirectional data flow in the entire network. In the downlink direction, the OLT broadcasts the service data from the metro and backbone networks to the ONUs through the ODN. In the upstream direction, the OLT receives and separates the data stream from each ONU and forwards it to the upper layer networks. On the one hand, PON has an asymmetric structure so that the cost at the OLT side can be shared by all ONUs. On the other hand, the cost of an ONU needs to be covered by each customer. Therefore, it is necessary to ensure the cost-effectiveness in the ONU when making upgrade strategies.

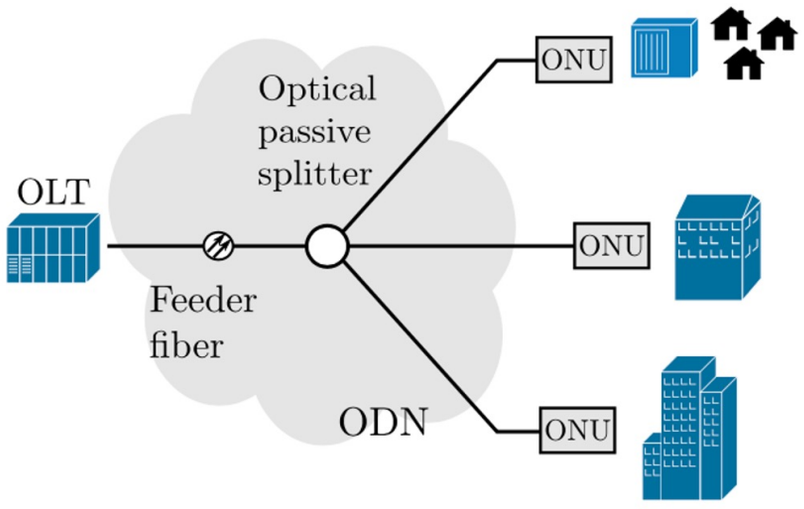

Figure 2.2: PON architecture.

2.2 Multiplexing technologies in PONs

Since the access network of PON is a PtMP structure, downlink data is broadcast over a single fiber to each ONU. Therefore, the data needs to be multiplexed and packaged according to certain rules for transmission and demultiplexed at the user side. Similarly, in the upstream direction, data from different ONUs are multiplexed into the same feeder cable and transmitted back to the OLT. The commonly used multiplexing techniques in PONs are time-division multiplexing (TDM), wavelength division multiplexing (WDM), and orthogonal frequency division multiplexing (OFDM).

TDM-PON

TDM-PON is the most widely adopted technology in optical access networks. In the downlink, the OLT divides a frame with duration T into N time slots. Each slot belongs to an ONU. The Downstream data is broadcast to all ONUs via the passive splitters, and each ONU only receives the data from its own time slot and discards other time slots. In the upstream, the user sends data in a burst mode during the specific time slots that the OLT assigns to the ONU. Different wavelengths are used for the uplink and downlink. The uplink and downlink are separated by the circulator in both the OLT and ONU. Currently established standards such as EPON, GPON, 10G EPON, and XG-PON belong to the TDM-PON category.

WDM-PON

The WDM-PON assigns a pair of independent wavelengths to each ONU for transmitting and receiving data, respectively [30]. The maximum number of ONUs is determined by the number of available wavelengths. The biggest challenge for WDM-

PON is how to achieve colorless ONU [31]. The colorless ONU means the transmitter and receiver in each ONU have the flexibility on wavelength allocation so that they can be tuned to any assigned wavelength for communication. It is beneficial for operation purposes. Employing tunable lasers and receivers (e.g., tunable optical filer) is the simplest solution despite with a high cost. A seeded reflective transmitter is more cost-effective, while a WDM filter is required in the ODN. To support more ONUs connections, further compression of the wavelength spacing of transmission carriers can yield dense wavelength division multiplexing (DWDM) [32] or even ultra-dense wavelength division multiplexing (UDWDM) PONs [33]. The scaling in the number of carriers can also increase the capacity of PONs [34]. Time-and-wavelength-division multiplexing (TWDM) which combines TDM and WDM technologies, is first adopted in NG-PON2 standard [35]. By employing TWDM, technologies of 10 Gb/s transceivers can be reused in NG-PON2. However, a tunable transceiver is required in ONU to meet the requirements of colorless ONU.

OFDM-PON

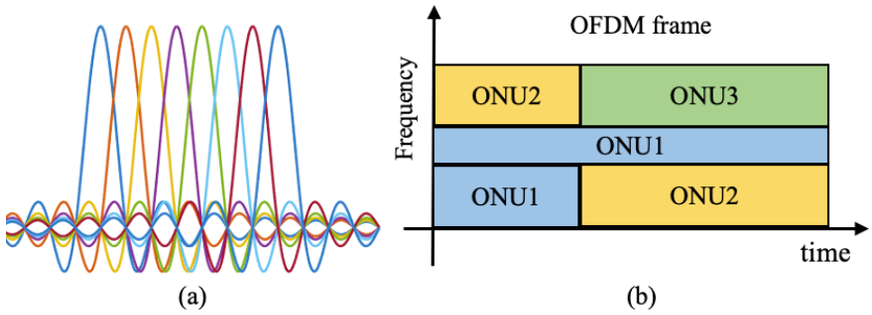

Figure 2.3: (a) OFDM spectrum; (b) An OFDM frame for downstream broadcast.

The OFDM is a multi-carrier modulation format, as shown in Fig. 2.3(a). It is widely used for high-speed optical transmission thanks to its superior physical layer performance [36]–[39], e.g., high-spectral efficiency and resilience to fiber dispersion. The OFDM-PON combines OFDM and TDM so that each OFDM subcarrier can be further split among different users in different time slots according to their demand, as shown in Fig. 2.3(b). Therefore, the OFDM-PON can allow a two-dimensional bandwidth allocation in terms of both time and frequency. Even with its flexibility and dispersion tolerance capability, because of the complexity and the corresponding cost of modulation and demodulation, it is mainly discussed in academia, and there is still a big gap from academia to commercialization.

2.3 PON evolution roadmap

The PON standard evolution has gone through several generations to satisfy the ever-increasing bandwidth demands per user. The different upgrade strategies are being proposed by industry, academic research institutions and finalized by international organizations. There are mainly three organizations for PON standardizations, namely, Full-Service Access Network (FSAN), ITU-T, and IEEE. The FSAN working group [40] was established in 1995 and now consists of 70 organizations from leading operators, equipment vendors, and Internet service providers. It is not a standard-setting body but helps to promote the development of ITU-T PON standards [41]. The ITU-T is known as the telecommunication standardization sector. APON/BPON, GPON, and NG-PON2 standards were all developed by FSAN and ITU-T [42]. The IEEE is an ISO-certified standards development organization, and its working groups have led the discussion of EPON and 10G EPON series of standards [43]. An essential requirement for different generations of PONs is compatibility, i.e., the new generation of systems can be compatible with the previous ones that are sharing the same fiber infrastructure. In addition to enabling the wholesale reuse of deployed fiber infrastructure, individual users should be able to evolve smoothly from the old system to the new one without the need to migrate all users forcibly all at once.

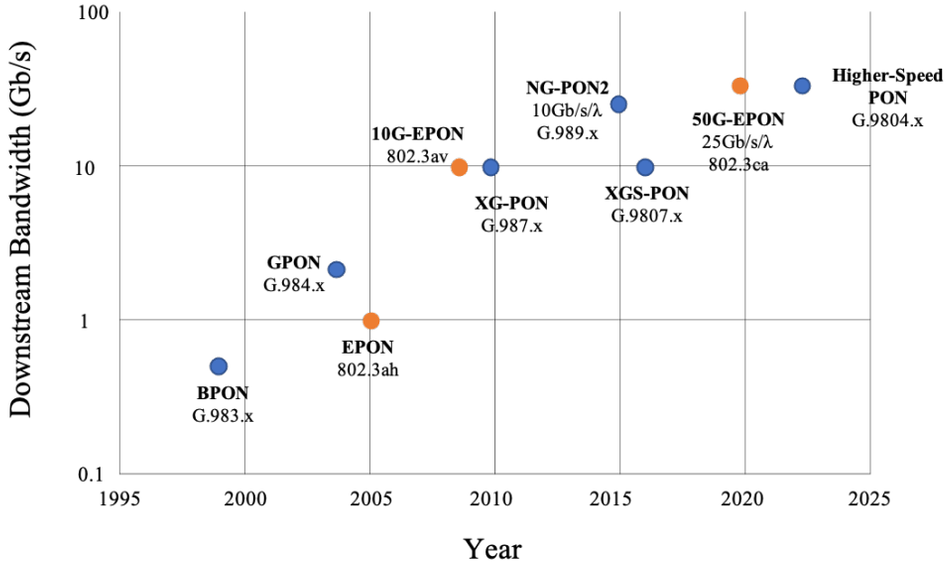

Figure 2.4: Roadmap of PON standardization [44].

Fig. 2.4 shows the roadmap of PON standardization, developed by ITU-T and IEEE, respectively. In the 1990s, the FSAN and ITU-T developed the first generation of APON standards based on asynchronous transfer technology (ATM) with a symmetric 155 Mb/s system speed, which was renamed as BPON after adding WDM technology [45], [46]. The APON and BPON standards are highly complex, and the ATM protocols are inefficient in supporting IP data services which could not

meet the growing demand for IP services. In 2004, IEEE completed the development of the Ethernet PON (EPON) 802.3ah standard, which specifies an upstream and downstream rate of 1.25 Gb/s [47]. The EPON replaces the ATM protocol with an Ethernet protocol, making the network more suitable for the IP service environment by supporting variable-length packet transmission. However, the EPON has low bandwidth utilization and also lacks effective support for real-time services. Subsequently, the FSAN/ITU-T introduced the gigabit PON (GPON) standard G.984 [48], which uses time-division multiplexing for upstream and downstream and supports variable rates up to 2.5 Gb/s and 1.25 Gb/s. GPON proposes a new frame structure, GPON encapsulation method (GEM), which provides a high quality of service for delay-sensitive voice, data, and video services. After that, the IEEE and ITU-T released PON standards with a system capacity of 10 Gb/s from 2009 to 2011: 10G-EPON [49], 10 Gb/s asymmetric XG-PON (X denotes 10) [50], and symmetric 10 Gb/s XGS-PON [51]. These standards also adopt the TDM-PON architecture and support symmetric and asymmetric transmission rates, which can reach 300 Mbps-1 Gbps per user on average. Currently, 10G-EPON and XG(s)-PON technologies are quite mature and will soon enter large-scale commercialization.

After the 10G PON, the route of the standard upgrade has been divided into two major directions. Direction one is to enhance the system rate directly by using the WDM technology. In 2015, ITU-T officially released the NG-PON2 standard [52], which adopted the TWDM-PON system architecture, transmitting 10 Gb/s signals per wavelength through four wavelength overlays, bringing the overall system rate up to 40 Gb/s. However, due to the cost of tunable optical components and system complexity, this standard has not been successful in actual commercial deployment and may be abandoned directly [53]. Direction two is to increase the rate of a single wavelength. Since 2015, the IEEE 802.3ca standards working group started a standard discussion for 25, 50, and 100 Gb/s PON, intending to increase the single-wavelength rate from 10 Gb/s to 25 Gb/s, and then to 50 Gb/s and 100 Gb/s through 2- and 4-wavelength multiplexing [54]. In July 2020, the IEEE officially announced the latest IEEE 802.3ca standard which removed the requirement for 100G rates and retained the single-wavelength 25G and two-wavelength 50G configurations. From 2018, the ITU-T also starts discussions for a single-wave rate 50 Gb/s higher-speed PON, and the standardization is expected to be completed by 2025 [42]. This thesis also follows this direction targeting on a low-cost solution for high-speed single-wavelength transmission.

2.4 Modulation formats in high-speed PONs

Modulation format selection is an important topic in high-speed PONs. The candidate modulation formats can be roughly divided into two categories: Single-carrier modulation and multi-carrier modulation. The single-carrier modulation is related

to the multilevel pulse amplitude modulation (PAM-M) formats such as NRZ-OOK, EDB or partial response system, and PAM-4. The representative of the multi-carrier modulation is DMT modulation, which is of higher spectrum efficiency together with higher complexity. In this section, the basics of these modulation formats and their application in PONs are presented.

2.4.1 Multilevel pulse amplitude modulation

PAM-M is a modulation format using different pulse amplitudes to represent data. The number of pulse levels M determines the spectrum efficiency and the decision complexity.

Non-return-zero on-off keying

The commonly used NRZ-OOK is a two-level PAM modulation. Each symbol represents only one-bit information. The time-domain waveform and eye diagram of NRZ-OOK are shown in Fig. 2-5. The OOK is a binary modulation, and the NRZ represents the signal amplitude would not drop into zero in the case of continuous high amplitude symbols. The NRZ-OOK signal is a binary stream, so symbol mapping or coding is unnecessary in the transmitter. In the receiver, a simple comparator can make symbol decisions and recover the original bits. In addition, unlike PAM-4 and DMT, the linearity of optoelectronic devices is not a big problem for the NRZ-OOK format since two amplitude levels are easy to be distinguished. Simple transceiver design and insensitive for the linearity are the reasons why the NRZ-OOK is the preferred choice of the legacy PON standards. One major drawback of the NRZ-OOK is the low spectrum efficiency. The required system bandwidth is close to the symbol rate. For the PON using 25 Gb/s NRZ-OOK, the costly 25G-class optics are required [55]. As the data rate increases to 50 Gb/s, the optical or digital compensation strategies are needed as techniques for 50G-class optics are far from the mature techniques [56]–[58].

PAM-4

The PAM-4 uses four different amplitude levels to deliver information, e.g., (−3, −1, 1, 3), where each symbol contains two bits of information. Compared to the NRZ-OOK, the PAM-4 with doubled spectrum efficiency can support the same bit-rate modulation with electronic components working at half speed. Moreover, the PAM-4 has higher tolerance to the fiber dispersion thanks to the doubled symbol period. However, the PAM-4 increases the linearity and signal-to-noise (SNR) requirements on optoelectronics to ensure equal space between different levels. It also requires a bit-symbol mapping from binary streams to the PAM-4 symbols at the transmitter side and a more complex decoder in the receiver. Despite the fact that increasing

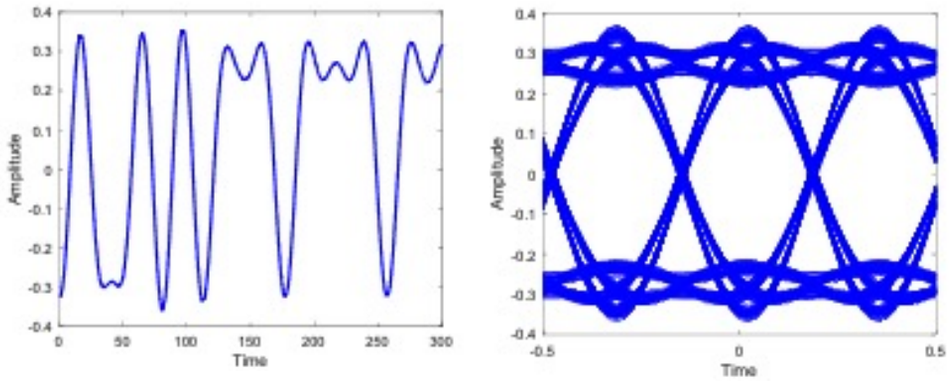

Figure 2.5: Time domain waveform of NRZ signal (a) and Eye diagram (b).

the number of amplitudes (e.g., PAM-8 or higher) leads to the improvement in bandwidth utilization efficiency, the difficulties on symbol decisions are also increased. Nevertheless, the 200/400G Ethernet standard already adopts PAM-4 as the modulation format [59], which is also preferred in 50G and 100G PON since the Ethernet industry chain and the optics can be reused [60].

Partial response system

The principle of a partial response system is to compress the signal spectrum by inducing controllable inter-symbol interference (ISI), letting one pulse spread to the neighboring ones. In this way, the duration of the pulse and hence the spectral efficiency are increased, enabling high-speed transmission under limited bandwidth. After transmission, the ISI can be removed by some techniques at the receiver side, and the original signal can be recovered. For the NRZ-OOK modulation, after a partial response system, the EDB with three amplitude levels can be obtained. Its spectral efficiency is similar to the PAM-4. Moreover, it is possible to use the partial response system for PAM-4 such that a seven-level duobinary PAM-4 (DB-PAM-4) could be generated, as can be seen in the eye diagram and spectrum of PAM-4 (Fig. 2.6 (a)(b)) and DB-PAM-4 (Fig. 2.6 (c)(d)).

Coding and decoding principle

Taking the PAM-4 as an example, the process of partial response operation can be done at the transmitter side by passing the PAM-4 symbols $s(k) \in \{-3, -1, 1, 3\}$ through a simple delay-and-add filter

$$r(k) = s(k) + s(k-1). \tag{2.1}$$

This operation connects adjacent symbols and makes each symbol lasting two

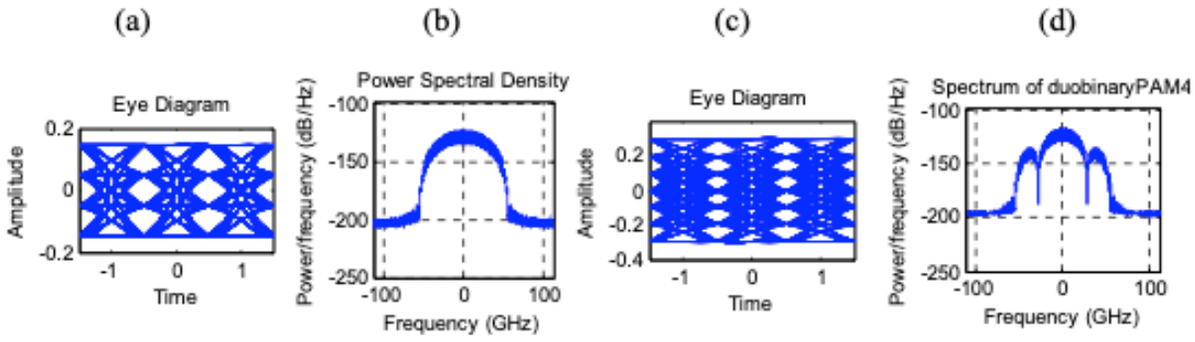

Figure 2.6: Eye diagram and spectrum of PAM-4 (a) (b) and duobinary PAM-4 (c) (d).

symbol periods. In this way, the input four-level signal can be transferred to a seven-level signal called DB-PAM-4 [61]. Also, in the receiver side, the easiest way to decode the DB-PAM-4 is to reverse the operation by

$$s(k) = r(k) - s(k-1). \tag{2.2}$$

Here, the decision result of each symbol would influence adjacent symbol decisions, resulting in error propagation. The pre-coding before the delay-and-add operation is employed to solve this problem [62],

$$b(k) = [s(k) - b(k-1)] \mod 4, \tag{2.3}$$

where $b(k)$ is the pre-coded PAM-4 symbols. After the partial response system, $b(k)$ is changed to seven-level DB-PAM-4 $c(k)$ following (2.4), and the original PAM-4 symbols can be recovered by

$$s(k) = c(k) \mod 4. \tag{2.4}$$

In the real applications, a partial response channel can be made by using the filtering effect from bandwidth limited optics. In a system where the 3 dB end-to-end bandwidth is around 25% of the signal baud rate, DB-PAM-4 can be generated. Although the DB-PAM-4 reduces the system bandwidth requirement, it is more sensitive to the nonlinearities and system noise.

2.4.2 DMT

The DMT modulation is widely investigated to increase the data rate in PONs in recent years. It can adaptively adjust the bit and power allocation of each sub-channel according to the channel quality. Then, the optimal modulation format and transmission rate can be applied accordingly. This section introduces the basic technologies about the DMT modulation, including quadrature amplitude modulation (QAM),

bit-power loading technologies.

Quadrature amplitude modulation

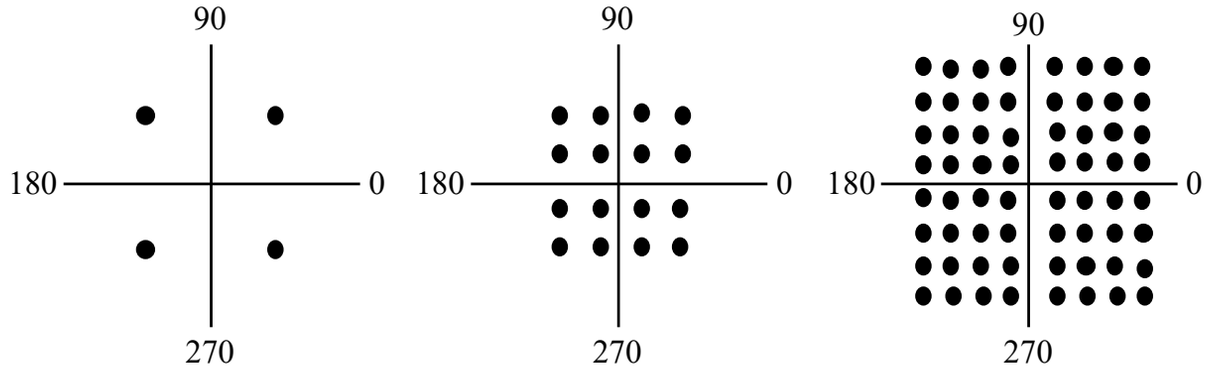

Figure 2.7: Constellation of 4 QAM, 16 QAM and 64 QAM.

DMT is a multi-carrier modulation technique, and each carrier is modulated with multiple QAM (QAM) symbols. QAM uses two orthogonal subcarriers to do amplitude modulation, and each MQAM symbol contains log2(M) bit information, so the spectrum utilization is doubled compared to the amplitude modulation. MQAM signal can be expressed by

$$C(t) = I_{\mathrm{m}} \cos w_{\mathrm{c}} t + Q_{\mathrm{m}} \sin w_{\mathrm{c}} t \tag{2.5}$$

where M is the modulation order ($M = 2^s$, s is the information bits in each symbol), I_{m} and $Q_{\mathrm{m}} \in \{1, 2, 3 \ldots M\}$, are the in-phase and quadrature components, respectively, and MQAM symbols can be mapped to a constellation diagram, shown in Fig. 2.7. In the constellation diagram, the minimum Euclidean distance indicates the noise tolerance. The larger the Euclidean distance, the better the noise tolerance can be.

Modulation and demodulation

Similar to the OFDM, the DMT is a multi-carrier modulation technique that divides the channel into several orthogonal sub-channels using the fast Fourier transform (FFT). The major difference between the DMT and OFDM is that the DMT does Hermitian conjugate symmetry before performing inverse FFT (IFFT) [63], [64], which transforms complex signal to real signal enabling amplitude modulation. Therefore, the DMT is an attractive solution in the PON system as it possesses many advantages of the OFDM without the need for coherent detection.

Fig. 2.8 shows the schematic diagram for DMT modulation and demodulation. The IFFT is used to convert the MQAM symbols $(c_0, c_1, \ldots, c_{n-1})$ into DMT signal

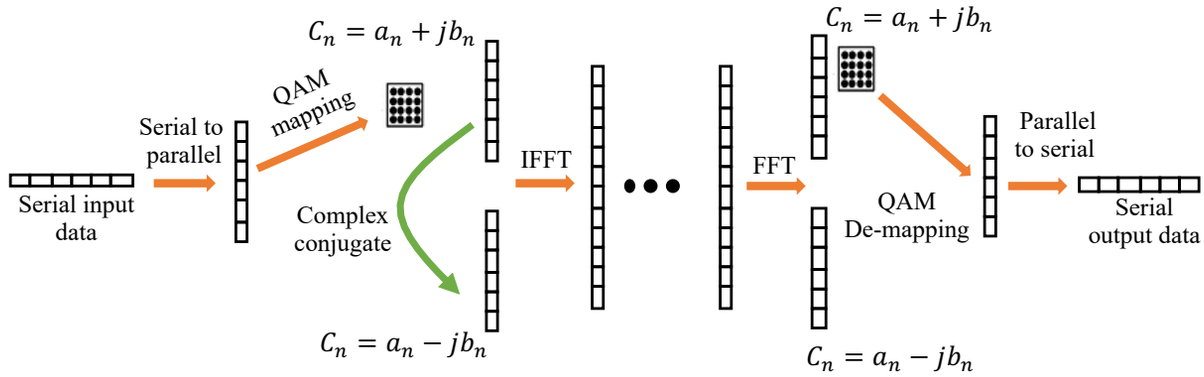

Figure 2.8: DMT modulation and demodulation scheme.

($P = \{P_o, P_1, \ldots, P_{n-1}\}$). Such a process can be expressed as

$$P_k = \sum_{n=0}^{N-1} C_n e^{j2\pi k \frac{n}{N}} = \sum_{n=0}^{N-1} C_n e^{j2\pi f_n t_k}, \tag{2.6}$$

with $k = 0, 1, \ldots N-1$. Define $f_n = \frac{n}{NT}$ and $t_k = kT$ where N is the total number of sub-carriers, T is the symbol period of the P_k. Eq. (2.6) represents the modulation of MQAM symbols in different subcarriers with frequency of $f_n = \frac{n}{NT}$. In this way, the frequency interval between sub-carriers is $\Delta f = \frac{1}{NT}$. The cross-correlation between any two sub-carrier S_l, S_m over one symbol period can be calculated as

$$\begin{aligned} \sigma_{l,m} &= \frac{1}{T}\int_0^T S_l S_m^* dt = \frac{1}{T}\int_0^T e^{j2\pi t(f_l - f_m)} dt \\ &= e^{j\pi(f_k - f_l)T} \frac{\sin\left(\pi\left(f_l - f_m\right)T\right)}{\pi\left(f_l - f_m\right)T}, \end{aligned} \tag{2.7}$$

where f_l and f_m are the carrier frequency of S_l, S_m. Since $f_l = af_m$ and a is an integer, $\sigma_{l,m}$ is always zero if $a \neq 1$. It means that all sub-carriers are orthogonal with each other. The corresponding frequency spectrum of DMT signal is shown in Fig. 2.9 (a). The DMT waveform in the time domain is random and irregular (see Fig. 2.9 (b)). Especially when most subcarriers with similar phases are superimposed, a DMT signal with a high peak- to-average power ratio (PAPR) affects the RF amplifier performance and increases the linearity requirement on optoelectronics. Note that the MQAM signals C_n with a length of $N/2$ are complex numbers at the beginning. In order to obtain a real-valued signal for intensity modulation, Hermitian conjugate $C_{N-n} = C_n^*$ is adopted, in which the length of IFFT is N. Hence, for a DMT based transmission system with a baud-rate of R_s, the signal bandwidth $B = N * \Delta f = R_\mathrm{s}$, and the real-valued bandwidth would be $R_\mathrm{s}/2$. In addition, to reduce inter-carrier interference and increase CD tolerance, the cycle prefix (CP), a sequence at the end of the symbols is copied and added to the beginning after the IFFT. In the receiver,

the reversed process with the FFT and MQAM de-mapping can be conducted for the DMT demodulation.

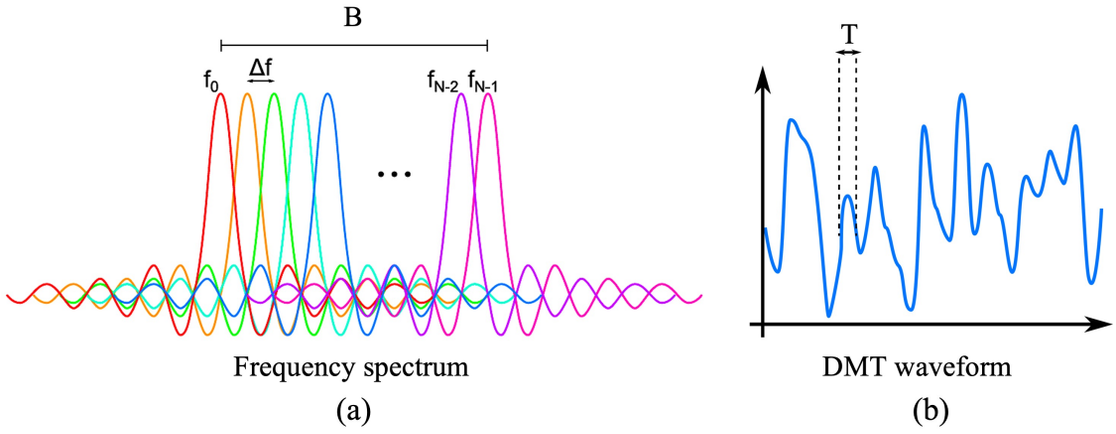

Figure 2.9: Frequency spectrum (a) and time domain waveform (b) of DMT signal.

Adaptive bit-power loading

Apart from the high spectrum efficiency, another advantage of using DMT is that it allows adaptive bit and power allocation according to the frequency response of the channel. This can be extremely beneficial in a quasistatic and slow-varying channel where the SNR of each subcarrier can be measured at the receiver side. Based on the SNR estimation, it is possible to redistribute the power unequally among different carriers at the transmitter side [65]–[68]. For example, when allocating more power to the high-frequency carriers with more power attenuation, the SNR profile response can be flattened after the system transmission. It is also able to independently select the QAM modulation order modulated on each sub-carrier. For example, the sub-carriers with higher SNR are able to load more bits than those with lower SNR, as can be seen in Fig. 2.10.

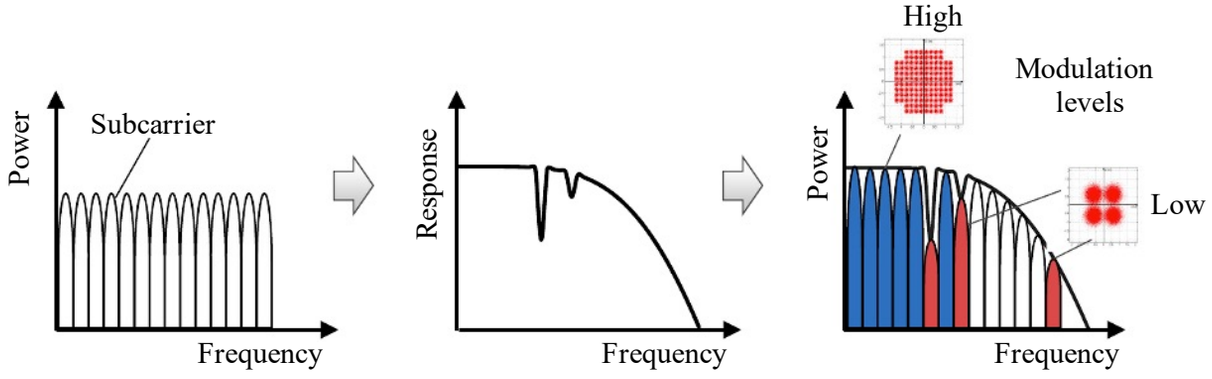

Figure 2.10: Adaptive power allocation and bit allocation.

2.4.3 Modulation formats for high-speed PONs

The NRZ-OOK is the simplest multilevel modulation format with the lowest requirements in pre-processing and post-processing among all discussed modulation formats. If 25G optics is standardized for 25G PON, NRZ should be the optimal choice. However, given that the upgrade plan is to reuse low-cost 10G optics, the EDB and PAM-4 are more promising formats than the DMT to replace the NRZ-OOK. It is because that the related technologies are more cost-effective and less disruptive than the DMT, while they still offer two times improvement in spectral efficiency compared to the NRZ-OOK. Sticking to the NRZ-OOK, requires external signal processing technologies, including OSP and DSP with relatively low complexity. In other words, the PAM-4 and EDB can provide capacity upgrade with minimal changes to the transceiver design because the deployed optoelectronic components do not need to be replaced.

Nevertheless, the DMT may become a good choice when the capacity increase to 50 Gb/s and beyond where the amount of the DSP required by the NRZ or PAM4 could be equivalent to the DMT requirements. The intensive DSP may include pre-equalization, post-compensation, and decoding algorithms for higher data rate transmission with PAM-4. While for the DMT, high-resolution ADCs, digital-to-analog converters (DACs), and linear modulators may also be required to support its strict linearity requirements. Therefore, if the main issue for the realization of 50 Gb/s is still the costly 25G optics, the simplified DSP may play a key role in future optical access networks.

CHAPTER 3

Impairments in PONs

The demand for the high-speed PONs puts new challenges on the physical layer design. System impairments need to be well addressed in a cost-effective way to meet the desired performance. The impairments in an intensity modulation and direct detection (IMDD) PON system are mainly coming from optoelectronics components and fiber. This chapter presents impairments most relevant to PONs including bandwidth limitation from transceivers, chirp effect from the directly modulated laser, pattern effect from SOA, and fiber transmission impairments.

3.1 IMDD system model

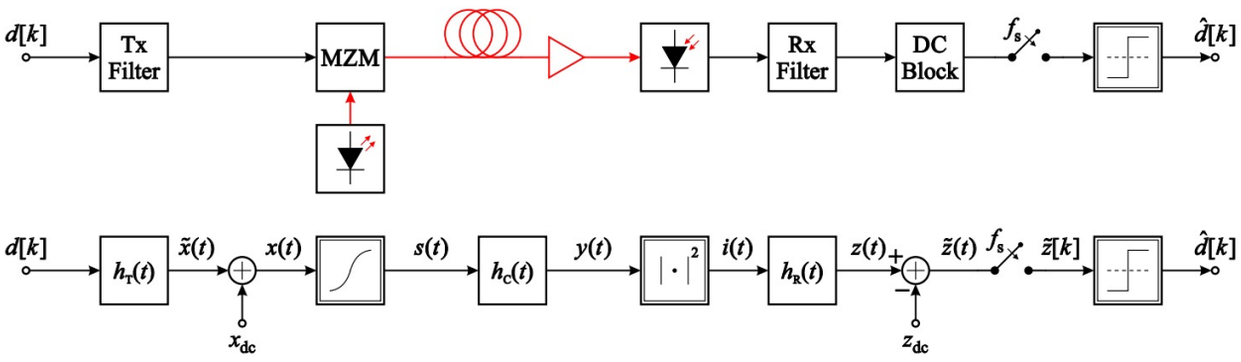

Figure 3.1: A block diagram of the IMDD system. This image is taken from [69].

The IMDD is a promising solution for PONs due to its cost-effectiveness [70].

Fig. 3.1 shows a block diagram of an IMDD system. $d[k]$ is the original discrete symbols. The signal $\tilde{x}(t)$ is generated from $d[k]$ after going through a pulse shaping filter $h_{\mathrm{T}}(t)$ [71]

$$\tilde{x}(t) = \sum_{k=-\infty}^{+\infty} d[k] h_{\mathrm{T}}\left(t - k t_{\mathrm{b}}\right), \tag{3.1}$$

where t_{b} is the symbol interval. Then $\tilde{x}(t)$ combined with a direct current (DC) bias enters the intensity modulator to realize the electro-optical conversion, the output can be expressed as

$$s(t) = \tilde{s}(t) + s_{\mathrm{dc}}, \tag{3.2}$$

where $\tilde{s}(t)$ is the transmitted signal without DC, and s_{dc} is the DC bias term. After the fiber transmission, the output of the signal after the PD detection is

$$i(t) = y_{\mathrm{dc}}^2(t) + |\tilde{s}(t) \otimes h(t)|^2 + 2 y_{\mathrm{dc}} \tilde{s}(t) \otimes \mathcal{F}^{-1}\{\mathrm{Re}\{H(f)\}\}, \tag{3.3}$$

where $\otimes$ denote the convolution operation, $h(t)$ is the inverse Fourier transform of the system response $H(f)$, consisting of the transmitting filter response $h_{\mathrm{T}}(t)$, the fiber response $h_{\mathrm{C}}(t)$, and the receiving filter response $h_{\mathrm{R}}(t)$, denoted as

$$h(t) = h_{\mathrm{T}}(t) \otimes h_{\mathrm{C}}(t) \otimes h_{\mathrm{R}}(t). \tag{3.4}$$

The first term in (3.3) is the DC component, which does not contain valid information and can be completely filtered out by a DC blocker. The second term is the nonlinear crosstalk introduced by the square detection, i.e., signal-signal beat interference (SSBI) [72]. The third term is the target term for the signal recovery.

For simplicity, we ignore the SSBI and assume that the optical power launching into the fiber is low that the overall system response can be considered as a linear low-pass filter. In this way the original signal recovered from the third term can be expressed as

$$i'(t) = \sum_{k=-\infty}^{+\infty} \tilde{d}[k] h\left(t - k t_{\mathrm{b}}\right). \tag{3.5}$$

After sampling and decision, we can obtain the original symbols as

$$i'\left(t_m\right) = \tilde{d}[k] + \sum_{k=-\infty, k\neq m}^{+\infty} \tilde{d}[k] h\left(t_m - k t_{\mathrm{b}}\right). \tag{3.6}$$

The first term in (3.6) is the mth symbol, and the second term is the ISI due to the nonideal system response $h(t)$. Considering the nonlinearity of modulators and fiber, both linear and nonlinear ISI are included in (3.6). Sec. 3.2 will introduce the major impairment sources resulting in the imperfect system response.

3.2 Optoelectronics impairments

3.2.1 Bandwidth limitation

The bandwidth of the optoelectronics components in the optical transmission system determines the maximum transmission rate that the system can support. The frequency response of a bandwidth-limited channel can be regarded as a linear low-pass filter, as expressed in (3.5). When a high-speed signal passes through the filter, the original symbols are broadened and overlap, causing ISI. According to the Nyquist Theory, a signal with a symbol rate of 1/T requires a minimum system bandwidth of 1/2T for an ISI-free transmission [73]. While in the practical applications, the thermal noise limit in the system increases the the required bandwidth to 2/3T or even 1/T to completely mitigate the influence of ISI [74].

As mentioned in Chapter 2, if the NRZ-OOK format is used, the high cost of 25G-class optical components is the most significant limitation to the NRZ-OOK deployment for 25G PON [75]. A cost-effective solution is to reuse the off-the-shelf 10G optoelectronic components [76]–[79]. Then, the OSP or DSP is needed for signal distortion compensation due to the limited bandwidth. In [77], 10G optics is proposed for 25 Gb/s NRZ transmission. The narrow optical filtering based on the delay interferometer is employed for bandwidth improvement. The disadvantage of this method is that it is sensitive to wavelength drifting. In [80], digital pre-distortion and Faster-than-Nyquist algorithms are proposed to compensate for the bandwidth limitation. Even these methods can help achieve good performance, the DSP cost is the biggest disadvantage. An alternative solution is to use spectrum efficient modulation formats such as the EDB [81]–[84] and PAM-4 [85]–[87], but at the cost of increased decision complexity and requirements on the system linearity. Bandwidth limitation becomes more serious in 50G PON and 100G PON, in which the DSP combined with the PAM-4/EDB/DMT is the normal solution [88]–[91].

3.2.2 Modulation nonlinearities

In an IMDD system, an optical modulator in the transmitter is used to modulate the optical carrier with the electrical signal. The linearity of the modulator makes a significant influence to the transmission performance. Fig. 3.2 (a) shows an example of PAM-4 modulation with a Mach-Zehnder modulator (MZM). The linearity of the modulation curve influences the interval between different levels and determines the quality of the eye diagram. To relieve the modulation nonlinearity, modulators with good linearity is necessary.

There are two categories of modulators for intensity modulation: External-modulation based external modulators and direct modulation-based DMLs [92], [93], as shown in Fig. 3.2(b). External modulation is composed of a laser source and an external modulator. The typical external modulators are electro-optical modulator (EOM)

[94], electro-absorption modulator (EAM) [95], and MZM [96]. External modulators have the advantages of large bandwidth, small modulation chirp, and better linearity, which are suitable for high-speed, long-reach transmission with advanced modulation formats. However, external modulators suffer from high insertion loss, so that an optical amplifier is usually needed. For the direct modulation, it is conducted by changing the driving current of the laser with the modulation signal. Compared with the external modulation, the system complexity and cost of the direct modulation scheme are much lower. The DML family includes a group of lasers such as vertical cavity surface-emitting laser (VCSEL) [97], [98], Fabry-Perot (FP) laser [99], [100], and distributed feedback (DFB) laser [101], [102]. Despite the lower cost, the linearity of the DML is not as good as the external modulators.

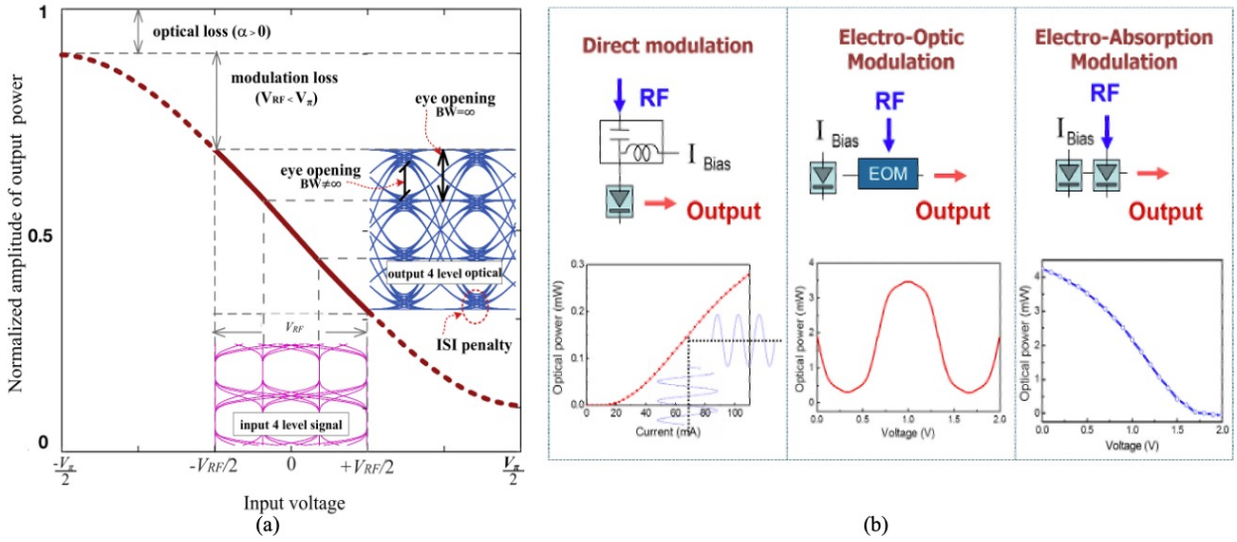

Figure 3.2: An example of PAM-4 signal modulation with MZM (a) and the schematic diagrams and modulation curve of DML, EOM and EAM (b). This image is taken from [92].

3.2.3 DML chirp

With the advantages of single longitudinal mode, narrow linewidth, and high output power, DFBs are used as an important light source in optical communications. Directly modulated DFB lasers-based IMDD systems are widely discussed in optical access networks since high-speed transmission can also be achieved by direct modulation rather than using expensive external modulators. However, DMLs are directly modulated by changing the injection currents, which also affects the carrier density inside the laser, resulting in the change of the refractive index in the active region and output wavelength drift. The wavelength drift is also known as frequency chirp, which broadens the signal spectrum after propagation through dispersive fiber and limits the transmission distance. The frequency chirp $\Delta V(t)$ can be derived from the

laser rate equations expressed as [103]

$$\Delta V(t) = \frac{\alpha}{4\pi}\left(\frac{d}{d_t}\ln(P(t)) + \kappa P(t)\right), \tag{3.7}$$

where $P(t)$ is the laser output power, κ is the adiabatic chirp factor, and α denotes the linewidth enhancement factor. The first term on the right side of (3.7) is called transient chirp which leads to serious frequency modulation at the rising edge and falling edge of the optical pulse. The second term is the adiabatic chirp which appears with varied pulse power, i.e., '1' bits with blue shift and '0' bits with red shift.

When α is positive, the transient chirp is a monotonically increasing function with the logarithm of $P(t)$. Since $P(t)$ increases with the time at the rising edge of the pulse, the blue shift appears leading to the increase of the instantaneous frequency. From another perspective, $P(t)$ decreases with time at the falling edge, causing the fact that the red shift is a result of reduced instantaneous frequency. When α is negative, the opposite phenomenon can be observed, as shown in Fig. 3.3.

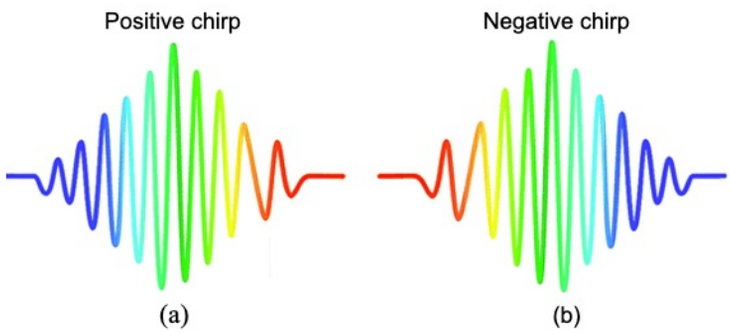

Figure 3.3: Optical pulse with positive chirp (a) and negative chirp (b).

For standard single-mode fiber (SMF), the dispersion at 1550 nm is positive. The group velocity of an optical pulse decreases with the increase of instantaneous frequency during the propagation along the fiber. For the optical pulse with positive chirp, the falling edge transfers faster than the rising edge, leading to a broadened pulse and ISI among adjacent symbols. This is why C-band DML is rarely used in long-reach communications. Using optical filtering [104]–[106] or chirp-managed laser [107] can help to compress the chirp in the optical domain but require a wavelength alignment. Some research groups also propose to use DML chirp to achieve complex modulation [108], [109], while this scheme is sensitive to temperature and coherent detection is needed in the receiver.

The phenomenon is opposite if the fiber link is with negative dispersion. The optical pulse with positive chirp can be compressed [110], [111]. Therefore, if there exists an amount of negative dispersion in the system, the DML chirp can balance the total dispersion and improve the transmission performance. By exploiting the interaction between chirp and dispersion, it is possible to achieve bandwidth compensation

for the system. Based on this idea, dispersion-supported equalization technology is proposed and described in Chapter 5.

3.2.4 Pattern effect in SOA

Optoelectronics with large bandwidth and high receiving sensitivity are necessary for 100G PON to ensure enough power budget (>29 dB). The commercial 25G APD is not yet mature for massive production. An alternative is to use a pre-amplifier combined with PIN-PD [112]. The PIN-PD with low sensitivity but large bandwidth is widely used in data center application. With the high volumes in 100G data center interconnects, 25G PIN-PD has become mature and cost effective enough to be adopted for 100G PON [70]. For the pre-amplifier, the SOA with a simple structure, low power consumption, and easy integrability with photonics circuit, is preferable for PONs compared to costly erbium-doped fiber amplifier (only in C-band) and Raman amplifier. The problem with SOA is the nonlinear pattern effect induced by the gain saturation. Since PON is with a PtMP structure, the receiving power for different users is different. The closest user with high receiving power leads to SOA saturation which may degrade the overall receiving performance. Therefore, the receiving power range is limited, known as receiving dynamic range [113].

The SOA gain G is the ratio between output power P_{out} and input power P_{in}. With the increase of SOA input power, G could be saturated since carriers deplete inside the active region [114]. The relationship between G and P_{out} can be denoted as [115]

$$G = G_0 e^{\left(-\frac{G-1}{G}\right) * \frac{P_{\text{out}}}{P_{\text{sat}}}}, \tag{3.8}$$

where G_0 is the small signal gain, and P_{sat} is the saturation output power defined as the output power at which G is 3 dB less than G_0. P_{sat} is the threshold between linear and nonlinear regions. When $P_{\text{in}} \ll P_{\text{sat}}$, $\left(-\frac{G-1}{G}\right) * \frac{P_{\text{out}}}{P_{\text{sat}}}$ would get close to 0 by replacing P_{out} with GP_{in}. Then we can get $G \approx G_0$ and the SOA works as a linear amplifier. As the increase of P_{in}, G decays exponentially. Fig. 3.4 shows the measured $G - P_{\text{out}}$ curve of the SOA. It can be observed that the SOA saturation output power is 7 dBm and it begins to saturate when the input power is higher than -13 dBm.

After signal modulation, G becomes time-dependent due to the instantaneous power of input pulse. Then, the SOA instantaneous gain $G(t)$ can be denoted by

$$G(t) = \frac{G_0}{G_0 - (G_0 - 1)\, e^{(-E(t)/E_{\text{S}})}}, \tag{3.9}$$

$E(t)$ is the energy of input pulse at the range of $\tau < t$ and it can be expressed by

$$E(t) = \int_{-\infty}^{t} P_{\text{in}}(\tau) d_\tau. \tag{3.10}$$

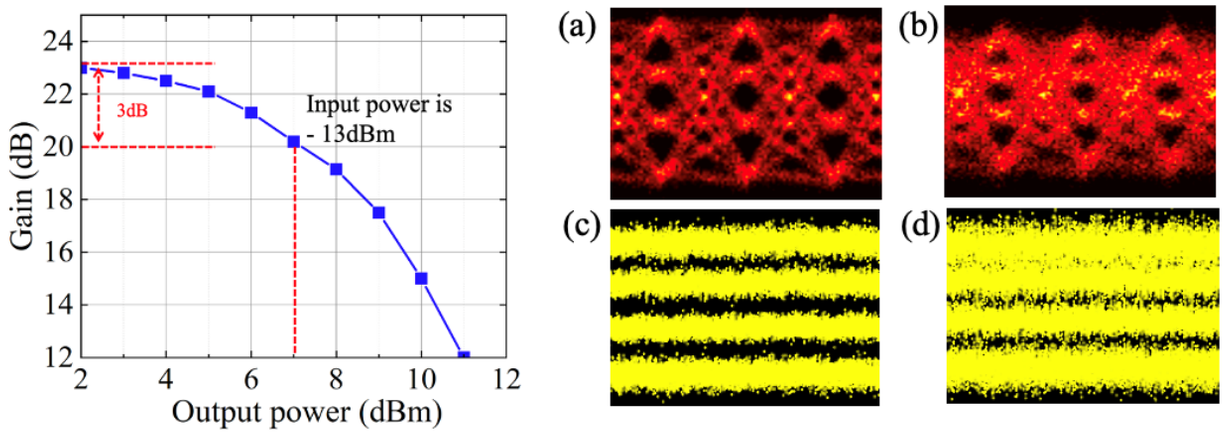

Figure 3.4: SOA gain versus output power. Insets (a) and (b): Eye diagrams of PAM-4 signal without and with SOA pattern effect, and Insets (c) and (d): PAM-4 signal symbols without and with SOA pattern effect. All eye diagrams are captured at the input power of −13 dBm.

In (3.9), E_s is the saturation energy. For an optical pulse with energy $E_g > E_s$, the SOA is not saturated at the leading-edge gain $G(-\infty) = G_0$. While for the tailing-edge, the gain changes to $G(\infty) = G_0/[G_0 - (G_0 - 1)e^{(-E_g/E_s)}]$. Therefore, the rectangle pulse evolves to jagged, and the gain decrease becomes worse with higher input power. Also, for a sequence of symbols with different power levels, the power level of the former symbol could also influence SOA gain to the current symbol, known as the SOA pattern effect. Insets (a)-(d) of Fig. 3.4 show the eye diagrams and symbol levels distribution without and with SOA pattern effect for PAM-4 signal, with an input power of −18 dBm and 0 dBm, respectively. It is clear that the pattern effect distorts the eye diagram, especially on the higher levels. Therefore, the SOA pattern effect needs to be compensated if it is employed as a pre-amplifier in the ONU. Gain-clamped SOA is an effective solution [116], nevertheless, it requires another laser source for external injection operating outside the signal band. Optical filtering [117], digital backward propagation [118], pulse shaping and probability shaping [119] can also help to alleviate this effect, but at the cost of high complexity.

3.3 Fiber impairments

The propagation of optical pulses along the optical fiber is subject to various effects that may change the original pulse shape and spectrum, thus affects the transmission performance of the communication system. These effects can be roughly classified as linear effects such as fiber attenuation, fiber dispersion, and nonlinear effects caused by Raman and Brillouin scattering. For PONs, the linear effects are usually more severe, especially with the increase of data rate and transmission distance. When the

optical power is high enough, the nonlinear effects can also distort the signal to an unrecognizable level. Both linear and nonlinear effects are discussed in this section.

3.3.1 Power attenuation

As the optical pulse propagates through the fiber, the optical power is reduced due to material absorption, Rayleigh scattering, and material impurities induced extrinsic absorption [120]. In the case of linear attenuation, the evolution of the optical power, $P(z)$, at the fiber length of z, is decided by Beer's law expressed as

$$P(z) = P(0)e^{-\alpha z}, \tag{3.11}$$

where $P(0)$ is the initial optical power at the input and β is the linear attenuation coefficient. As $P(z)$ decreases exponentially with the factor $e^{-\alpha z}$, β is usually expressed in dB per unit length by

$$\beta_{\text{dB}} = \frac{10}{z} \log\left(\frac{P(z)}{P(0)}\right). \tag{3.12}$$

The attenuation efficient β varies with the wavelength since the impure hydroxide ion that existed in the fiber has different absorption peaks. Fig. 3.5 shows the SMF attenuation profile for different operating wavelengths. The three communication windows for telecommunication applications are set to the wavelength range with low power loss. During the past years, fiber fabrication techniques have improved a lot. The value of β at 1550 nm can reach below 0.2 dB/km, which means that the optical beam is transmitted in the fiber with less than 4% optical loss per kilometer. For O-band at 1310 nm, this value increases to 0.3 dB/km.

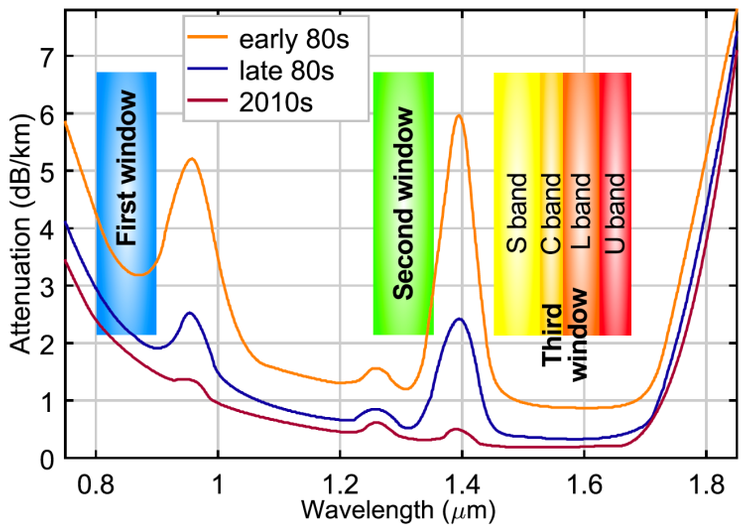

Figure 3.5: SMF attenuation versus operating wavelength. This image is taken from [121].

3.3.2 Dispersion

The velocity of the optical pulse depends on its frequency and mode during propagating along the optical fiber. The optical pulse usually contains multiple frequency and modes components, and these components transmit at different speeds leading to pulse broadening or compressing, which is so-called dispersion. There are various types of dispersion that existed in the optical fiber.

Modal dispersion

Modal dispersion (MD) only exists in multimode optical fiber. Multiple modes with different speeds activated when the optical pulse is propagating in the multimode fiber. The varying rates of these modes lead to the broadening of the optical pulse, which is known as MD. The MD is the key issue that needs to be solved for long-reach multimode transmission. Considering the low-cost and connection convenience, multimode fiber is widely used in short-reach interconnections. In PON, SMF with a small core diameter is used, which can only support the propagation of one fundamental mode, so MD can be neglected.

Chromatic dispersion

Chromatic dispersion (CD) can also broaden the transmitted optical pulse with single-mode transmission. CD comes from the frequency-dependent fiber refractive index making the different frequency components of a signal propagating in different velocity, which may cause the original optical pulse to expand in time, and the amount of expansion is determinate by the fiber length. Finally, ISI could be induced if the symbol broadens beyond its symbol period. In optical communication, the fiber CD is usually characterized by the parameter D [ps/(nm·km)] or β_2 [ps^2/km]:

$$D = -\frac{2\pi c}{\lambda^2}\beta_2 \tag{3.13}$$

$$\beta_2 = -\frac{1}{v_g^2}\frac{dv_g}{dw} \tag{3.14}$$

v_g is the group velocity and w is the angular frequency. The CD can be positive and negative depending on the value of D or β_2. From (3.14), it can be observed that v_g varies with the frequency if CD is non-zero. When $\beta_2 < 0$, or $D > 0$, v_g monotonically increases with w, which means higher frequencies are faster than low frequencies during fiber propagation. On the other hand, if $\beta_2 > 0$, or $D < 0$, higher frequencies have a lower propagation speed than lower frequency.

For SMF, D is approximately 17 ps/(nm·km) at 1550 nm (f = 193.4 THz). Dispersion is the major impairments for high-speed transmission, especially when the transmitted signal with positive chirp (as introduced in Sec. 3.2.3). To reduce the

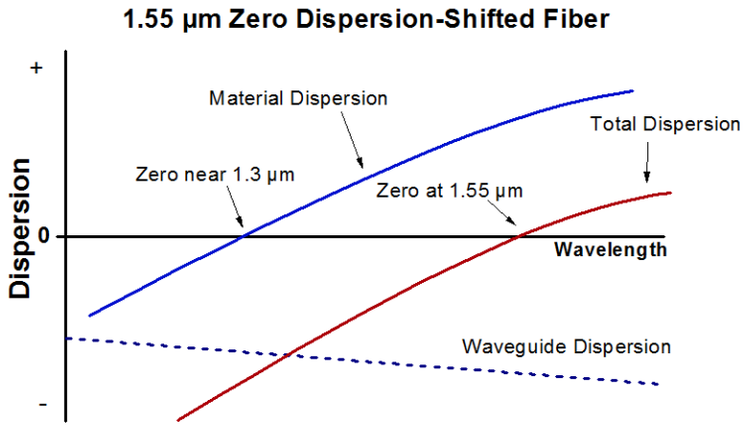

Figure 3.6: Dispersion profile of different fiber type.

CD effect, dispersion-shifted fiber (DSF) is designed to shift the zero-dispersion wavelength from 1300 nm in SMF to the minimum-loss window at 1550 nm, as shown in Fig. 3.6. An alternative solution is fiber Bragg grating (FBG) [122] or dispersion compensation fiber [123], which can produce negative dispersion in the C-band. Electrical dispersion compensation (EDC) is also an efficient method for CD mitigation [124]–[126], especially for coherent systems [127]–[129]. While for an IMDD system, CD cannot be efficient mitigated by EDC since the phase information is lost during square law detection.

Polarisation mode dispersion

Polarization mode dispersion (PMD) caused by fiber birefringence is another source of pulse broadening during optical pulse propagation along SMF [130]. There are usually two orthogonal polarization modes propagation in the SMF. Ideally, these two modes propagate in the x- and y-direction are with identical properties, making them indistinguishable. However, the random birefringence influences the refractive index experienced by two different polarization modes in actual cases. Then the velocity of these two modes would be different and cause pulse broadening. Random birefringence in optical fibers is caused by deformed core geometry during the imperfect manufacturing process, fiber stress, and bending, making it difficult to analyze in practice. Moreover, PMD becomes the major limitation for high-speed transmission when the system operates at a near-zero dispersion window of the fiber over long distances. The experiment results presented in this thesis with relatively low speed and short transmission distance, which make the PMD less important compared with other impairments such as CD.

3.3.2 Nonlinearities

Besides linear dispersion distortions, the fiber nonlinearities become significant if injected with high input optical power due to variation of the refractive index with the optical intensity. There are mainly three types of nonlinear effects during fiber transmission: Stimulated Brillouin scattering (SBS), stimulated Raman scattering (SRS), and Kerr nonlinearities. When the intensity of input pump light reaches a certain threshold, it would be partially converted into backscattered light due to the significant enhancement of the acoustic field by the electrostriction effect, which is known as SBS. The bandwidth of backscattered light is in the backward direction with only a few tens of MHz, and the center frequency is about 10 GHz lower than that of the input pump light. Therefore, SBS can be suppressed by broadening the optical bandwidth. DML-based IMDD PONs are often with a broad emission spectrum due to chirp, so the SBS effects are negligible during fiber transmission [105]. Then, for SRS, it is caused by the interaction between the incident light and the vibrational states of atoms in the fiber medium, which can also be neglected when the system with a single wavelength and low optical power. Finally, Kerr effect is related to the variation of fiber refractive index with optical power leading to the different effects according to the type of input signal, i.e., self-phase modulation (SPM), cross-phase modulation (XPM), and four-wave mixing (FWM). SPM and XPM are a conversion from intensity modulation to phase modulation when DML is used or launching power is higher than 10 dBm. XPM appears when multiple channels are transmitted in the fiber at the same time. The phase variation of a specific channel is dependent on the power intensity from itself and other channels. FWM often occurs when the wavelength of multiple channels is close to zero dispersion window of the fiber.

CHAPTER 4

Optical signal processing

There are commonly two solutions to address the system impairments meeting the performance requirement of 25G PON, employing 25G optoelectronics components with simple NRZ-OOK format, and using low-cost 10G optics together with EDB or PAM-4 format and DSP, as shown in Fig. 4.1 (a)(b). Using high-speed components is relatively expensive, and the old generation of devices cannot be reused. DSP requires high-speed DACs, ADCs, and complex multiplication circuits. Both DSP and high-speed components can lead to increased costs, being a severe concern for cost-sensitive subscribers. Alternatively, OSP can improve the signal quality directly in the optical domain without the need for optical-to-electrical (O/E) and electrical-to-optical (E/O) conversion (see Fig. 4.1 (c)). For example, use dispersion compensation fiber [131] or FBG [132] for dispersion compensation, employ optical filtering [133] or FWM effect [134] for chirp compression, and also make use of SBS for narrowband optical filtering [135]. This chapter introduces two OSP schemes, namely DSE and injection locking, for bandwidth improvement and chirp management. The DSE principle and application in 25G PON underlying **Paper A-C** are introduced and discussed.

4.1 Dispersion supported equalization

The chirp signal interacts with dispersion during transmission along with the fiber, shifting the chirp and dispersion-induced phase modulation to intensity modulation, thus affecting the overall system's frequency response. By exploiting this interaction

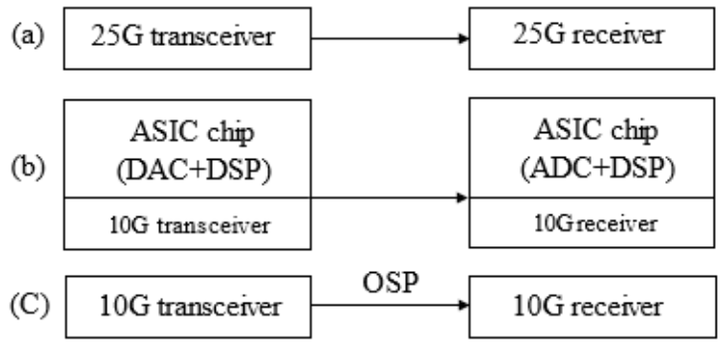

Figure 4.1: 25G PON based on (a) 25G optics, (b) 10G optics and DSP, and (c) 10G optics with OSP.

between chirp and dispersion, DSE technology is proposed for bandwidth improvement in the optical domain, and then electrical signal processing can be avoided.

4.1.1 Interplay between DML chirp and chromatic dispersion

Chapter 3 explains why the optical pulse from the DML can be compressed when transmitting over fiber with accumulated negative dispersion. This section through theoretical derivation further validates that the interaction between the DML chirp and negative dispersion can increase the system bandwidth.

As described in (3.7), the DML chirp can be considered as frequency modulation (FM) generated together with the amplitude modulation (AM) due to the complex susceptibility of the gain medium in the DML. The conversion from AM to FM can be described by [136]

$$F_{\text{in}}(jw) = \frac{\alpha}{2}(jw + \Gamma)\frac{1}{P_0}S_{\text{in}}(jw), \tag{4.1}$$

where P_0 is the average output power without signal modulation, Γ being the damping rate, α referring to the linewidth enhancement factor, and $S_{\text{in}}(jw)$ and $F_{\text{in}}(jw)$ are the response function of amplitude and frequency modulation, respectively. When transmission along the SMF, AM and FM convert to each other due to the interplay effect between chirp and dispersion. The mutual conversion matrix can be expressed as

$$\begin{pmatrix} S_{\text{out}}(jw) \\ F_{\text{out}}(jw) \end{pmatrix} = \begin{pmatrix} \cos\left(w^2\theta\right) & \frac{2jP_0\sin\left(w^2\theta\right)}{w} \\ \frac{jw\sin\left(w^2\theta\right)}{2P_0} & \cos\left(w^2\theta\right) \end{pmatrix} \cdot \begin{pmatrix} S_{\text{in}}(jw) \\ F_{\text{in}}(jw) \end{pmatrix}, \tag{4.2}$$

where θ is defined as $D\lambda^2 w^2 l/4\pi c$, D is the dispersion coefficient, λ refers to the wavelength, l denotes the fiber length, and c is the vacuum light speed, $S_{\text{out}}(jw)$ and $F_{\text{out}}(jw)$ express the output amplitude and frequency response function.

By substituting (4.1) into (4.2), the transfer function of fiber can be obtained

expressed as

$$\begin{aligned} G(jw) &= \frac{S_{\text{out}}(jw)}{S_{\text{in}}(jw)} \\ &= \sqrt{1+\alpha^2}\cos(\theta+\arctan(\alpha)) + j\frac{\alpha\kappa P_0}{w}\sin(\theta). \end{aligned} \tag{4.3}$$

The first and the second term in (4.3) reflect the power fading effect induced by the transient and adiabatic chirp of the DML, respectively. The power fading induced by the zero points in the spectral can be calculated by setting $\theta+\arctan(\alpha) = \pi/2+n\pi$ in the first term, and $\theta = \pi/2+n\pi$ in the second term considering the feature of the cosine and sine function. The total frequency response can be expressed as

$$|G(jw)| = \sqrt{(1+\alpha^2)\cos^2(\theta+\arctan(\alpha)) + \left(\frac{\alpha\kappa P_0}{w}\right)^2 \sin^2(\theta)}. \tag{4.4}$$

4.1.2 Enhanced bandwidth with negative dispersion

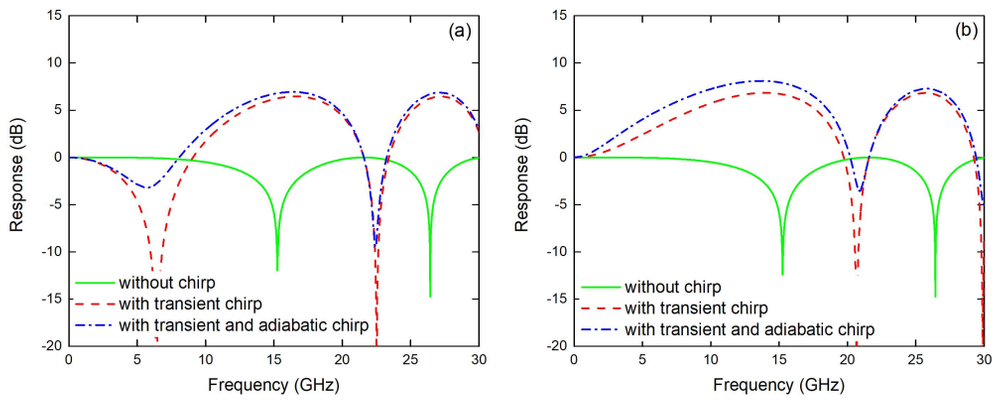

Figure 4.2: Theoretically calculated frequency response curves of SMF with (a) 320 ps/nm and (b) -320 ps/nm dispersion at 1550 nm.

Based on (4.4), the frequency response curves of dispersive fiber considering three different chirp settings are drew: 1) With both transient and adiabatic chirp, 2) with only transient chirp, and 3) without chirp. α and κ are set to 3.5 and 13 GHz/mW accordingly if chirp is considered. The accumulated dispersion is set to 320 ps/nm and -320 ps/nm by changing the sign of the CD coefficient. The theoretically calculated power fading curve of fiber under the parameter settings is shown in Fig. 4.2. It can be observed that the transient chirp further moves the first power dip, induced by the fiber dispersion, from 15 GHz to 6 GHz when the fiber is with positive dispersion. The power notch can move up to 20 GHz if negative dispersion is applied, and the power of high-frequency components can also be improved. Based on this result, it can be concluded that the power of high-frequency components can be increased

by using an amount of negative dispersion when the high-speed signal is directly modulated and detected by bandwidth-limited optical components, which is the so-called DSE. An experimental demonstration of 4×25 Gb/s NRZ-OOK signal with 10G optics in both O-band with DSE are presented in **Papers A** and **B**, proving the effectiveness of DSE.

4.1.3 Demonstration of symmetric 4×25 Gb/s PON with DSE

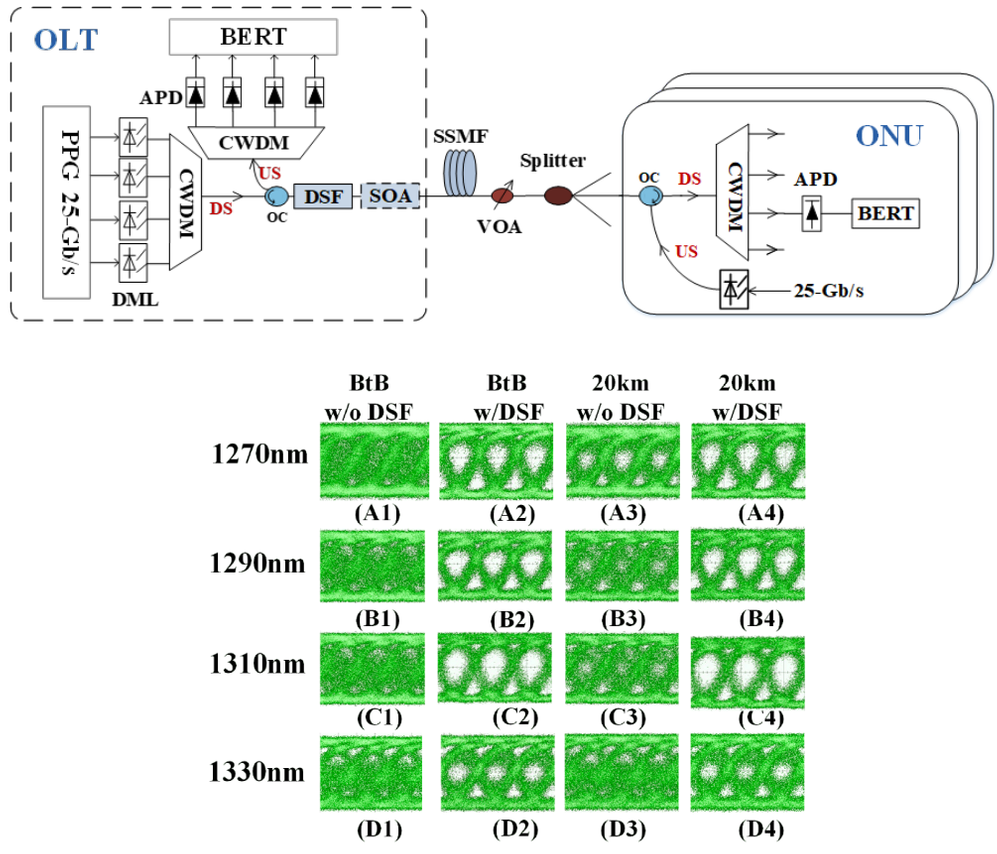

Figure 4.3: (a) Experiment setup for O-band symmetric 4×25 Gb/s PON with 10G optics, (b) eye diagrams of 25 Gb/s NRZ-OOK signals from four channels with and without DSF.

The system schematic diagram of a symmetric 4×25 Gb/s PON system with 10G DMLs and APDs in the O-band based on DSE is illustrated in Fig. 4.3 (a). Four commercial 10G DMLs operating at 1270 nm, 1290 nm, 1310 nm, and 1330 nm are used for 25 Gb/s NRZ-OOK signal modulation. The same waveband but with 200 GHz wavelength deviation are selected for four upstream channels. A spool of 10 km DSF with a total dispersion of −150 ps/nm at 1310 nm is employed for DSE function for both downstream and upstream channels to compensate for the bandwidth limitation. Considering DSF with an insertion loss of 10 dB, an SOA is employed to increase the launching power downstream and the receiving sensitivity

upstream. The eye diagrams of 25 Gb/s NRZ-OOK signal reopen with the help of DSF, enabling real-time detection without the need of DSP, shown in Fig. 4.3 (b). The performance of 1270 nm and 1330 nm channels is a little worse than 1290 nm and 1310 nm because the total negative dispersion value is not optimal for both of them. Finally, the system power budget at 1310 nm can achieve 26 dB and 32 dB for downstream and upstream, respectively.

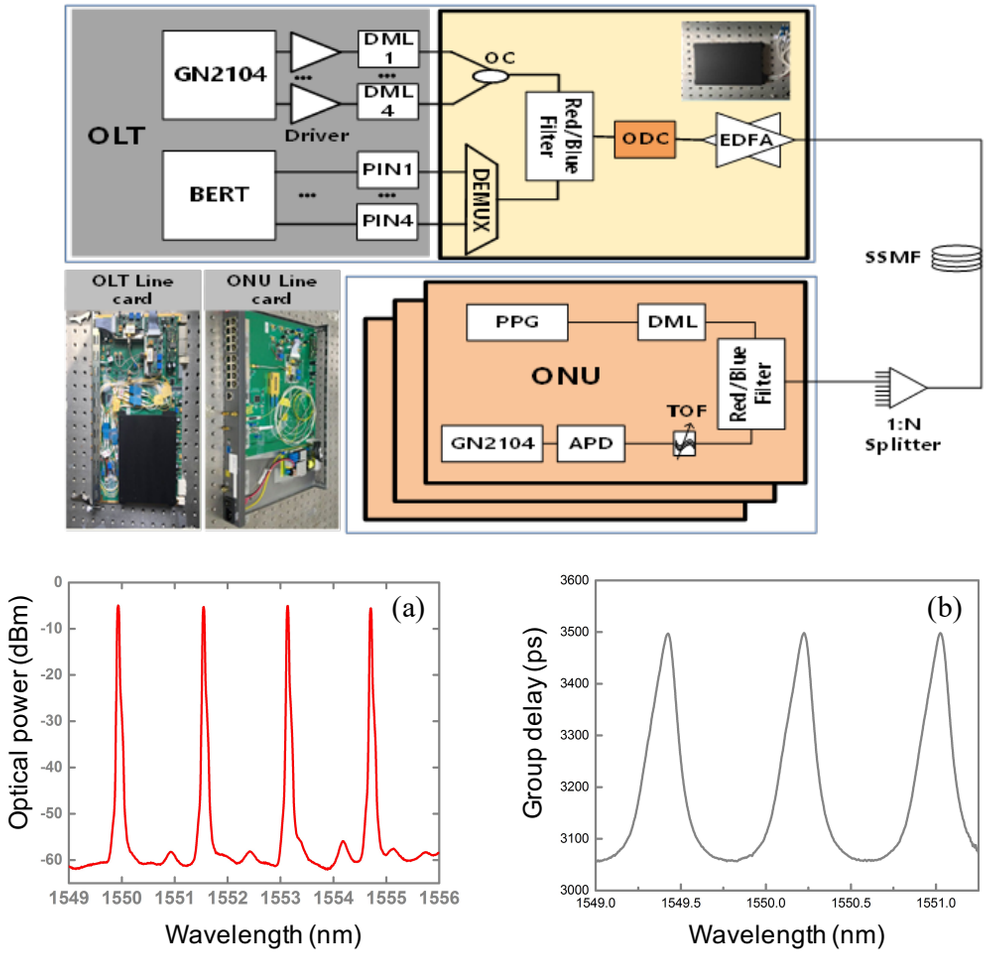

Figure 4.4: Experiment setup for C-band symmetric 4×25 Gb/s PON with 10G optics. Inset: (a) optical spectrum of four channels in downstream; (b) the measured group delay curve of ODC module.

The result presented above is demonstrated in the O-band. DSE also works effectively in the C-band, presented in **Paper C**. The experimental configuration is shown in Fig. 4.4. For downstream, four DMLs operating at 1549.96∼1554.74 nm with 200 GHz wavelengths spacing are employed as transmitters, each carrying 25 Gb/s NRZ-OOK signals. The spectral is shown in Fig. 4.4 (a). And the four upstream wavelengths are operated at 1538.98∼1541.35 nm with 100 GHz channel spacing, a red/blue filter separates the downstream and upstream signals. A multi-channel tunable optical dispersion compensator (ODC) with a channel spacing of 100 GHz

(see Fig. 4.4 (b)) is employed to provide negative dispersion for all channels. Since the SMF generates positive dispersion in C-band, the ODC needs to provide enough negative dispersion, responsible for both the CD compensation and DSE function.

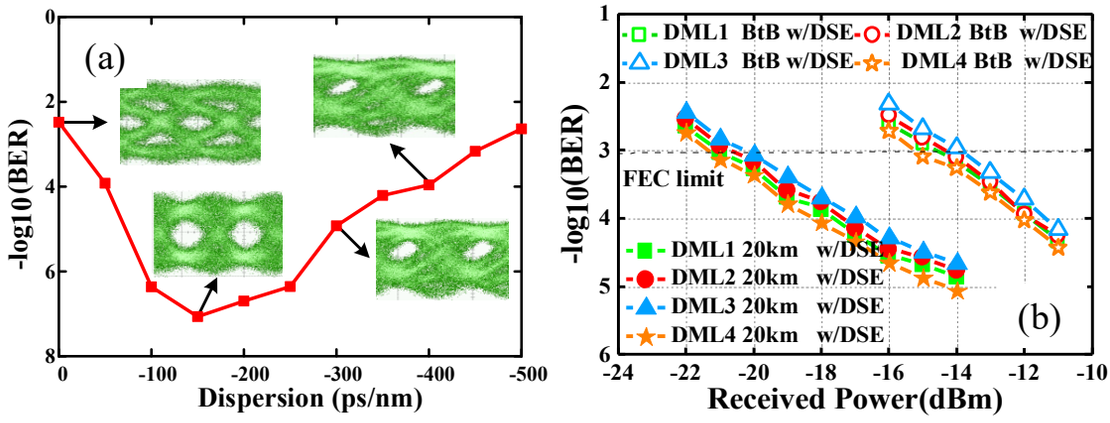

Figure 4.5: (a) BER measurement of 25 Gb/s NRZ-OOK signal under different negative dispersion value, (b) downstream transmission performance at BtB and 20 km SMF with DSE.

The system tolerance to the negative dispersion value in back-to-back configuration is measured, shown in Fig. 4.5 (a). The BER performance improves gradually at the beginning but degrades after the dispersion value exceeds −150 ps/nm. Compared with the 0 ps/nm case, the BER performance is continuously optimized when the negative dispersion value is within around −500 ps/nm. Since 20 km SMF in C-band introduces around 340 ps/nm dispersion value, the compensation value of ODC is set to −440 ps/nm considering the performance for users within the range from 0 to 20 km. The BER performance subject to different fiber lengths with DSE is presented in Fig. 4.5 (b). The sensitivity can achieve −21 dBm after 20 km SMF transmission with DSE. Considering the launching power of each channel being 16 dBm, the power budget could reach 37 dB. It is also observed that the receiver sensitivity at BtB is −15 dBm due to the over-compensated negative dispersion, corresponding to a power budget of 31 dB.

4.2 Injection locking

The modulation bandwidth of a DML is limited by its relaxation oscillation frequency, which can be partially improved by increasing the drive current. The relaxation oscillation frequency W_{R} can be obtained through the deduction from a three-rate equation which can be expressed by [137]

$$W_{\mathrm{R}} = \sqrt{\frac{v_{\mathrm{g}} a S_0}{\tau_{\mathrm{p}}}}, \tag{4.5}$$

where v_g is the group velocity, a is a constant, S_0 is the photon density, and τ_p denotes the photon lifetime. From (4.5), it can be observed that the laser's relaxation oscillation frequency increases with the photons density in the active region. The modulation bandwidth of the laser can be increased by external injection of photons, known as injection locking [138]–[140]. Today, injection locking is extensively investigated in the optical communication field. By cascading multiple injection-locked VCSELs, the modulation bandwidth can reach up to 100 GHz [141]. Thanks to the injection locking, the DML chirp can be compressed [142] and even altered from positive to negative enabling long-reach transmission [143]. Besides, injection locked-FP laser with larger wavelength tunability is a strong candidate for the colorless WDM-PON transmitter [144]–[146]. Some research groups also employ injection locking for radio over fiber transmission [147]–[149].

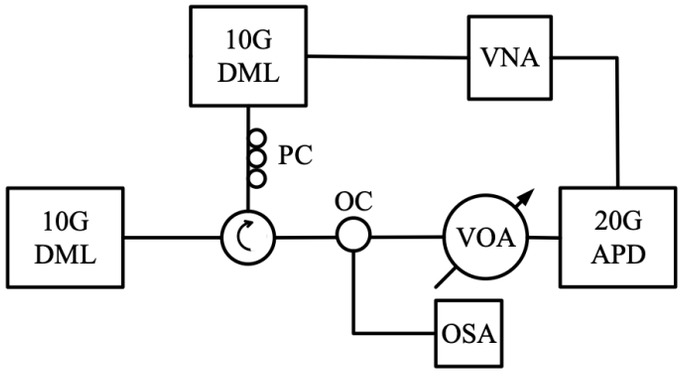

Figure 4.6: Experimental setup for frequency response measurement.

By taking advantage of injection locking for bandwidth improvement, it is possible to use low-cost 10G optics to achieve high-speed PONs. We experimentally measured the frequency response variation of the 10G DML in the presence of external light injection. The configuration of the experiment is presented in Fig. 4.6. The injection locking system consists of a master and slave laser (SL), where the master laser (ML) provides the external light source, and the SL is the one being injected. Both SL and ML are tunable DFB lasers. The wavelength interval between the ML and SL should be kept within a certain range to achieve stable locking. After locking, the operating wavelength of the SL follows the ML. An optical spectrum analyzer (OSA) is employed to monitor the locking condition, and a vector network analyzer (VNA) is used to measure the system bandwidth variation.

The SL can be locked when the wavelength interval is within 0.5 nm. The bandwidth evolution with and without injection locking is shown in Fig. 4.7. When 10G DML and 10G APD are used, the system bandwidth is about 10 GHz without injection locking. While after injection locking, the system bandwidth is improved to 15 GHz thanks to the increase of relaxation oscillation frequency, which is close to the bandwidth of a 20G-class device-based transmission system. With such higher

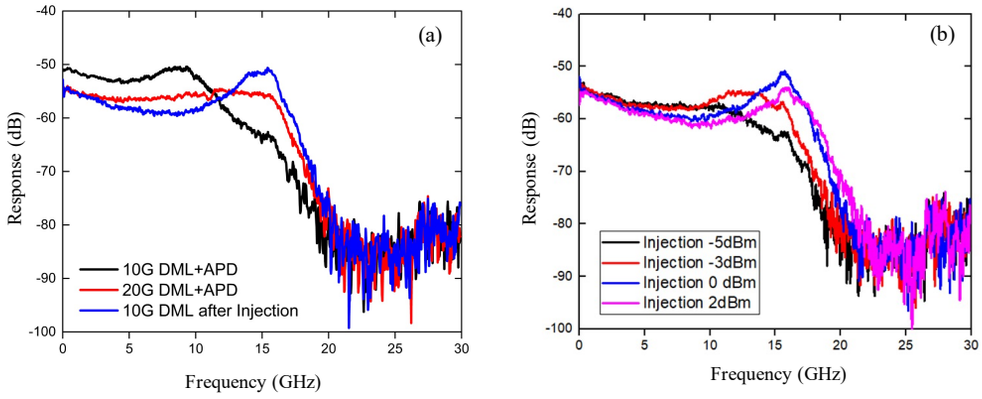

Figure 4.7: Measured system frequency response (a) with and without injection locking and (b) with different injection power.

bandwidth, 50 Gb/s signal transmission with advanced format is possible. Moreover, the relaxation oscillation frequency continues to increase with the increase of injection power, while the low-frequency response degrades. The optimal injection power needs to be further verified based on transmission performance, which is presented in **Paper H**. This part will be further introduced in Chapter 6.

CHAPTER 5

Digital signal processing

The DSP can mitigate linear and nonlinear distortions by manipulating the signal symbol by symbol in the electrical domain at both transmitter and receiver side, which is more flexible than the OSP introduced in Chapter 4. With the advanced development of complementary metal-oxide-semiconductor (CMOS), the cost of the DSP gradually may become acceptable for the IMDD PON, especially when the system capacity reaches up to 50 Gb/s or even 100 Gb/s [150].

Nevertheless, optimized DSP algorithms are still needed to reduce power consumption and cost, for instance, piecewise linear filtering [151] and simplified Volterra [152], [153]. Alternatively, the DSP cost can be reduced when moving the complex DSP module from each ONU (post-equalization) to the OLT (pre-equalization). In this way, the DSP cost is able to be shared by multiple ONUs. This chapter introduces the DSP algorithms with a focus on our proposed neural network (NN) based pre-equalizer and joint NTHP and Volterra equalization. The details of the work are presented in **Paper D** and **Paper E**.

5.1 Linear impairments compensation

5.1.1 FFE and DFE

In order to compensate linear and nonlinear impairments in the signal, the equalizer $W(f)$ can theoretically be designed to enable a full-pass response, i.e., the system frequency response after cascading is $H(f) \cdot W(f) = C$, as shown in Fig. 5.1(a) [154].

The most common type of equalizer is the forward feedback equalizer (FFE), shown

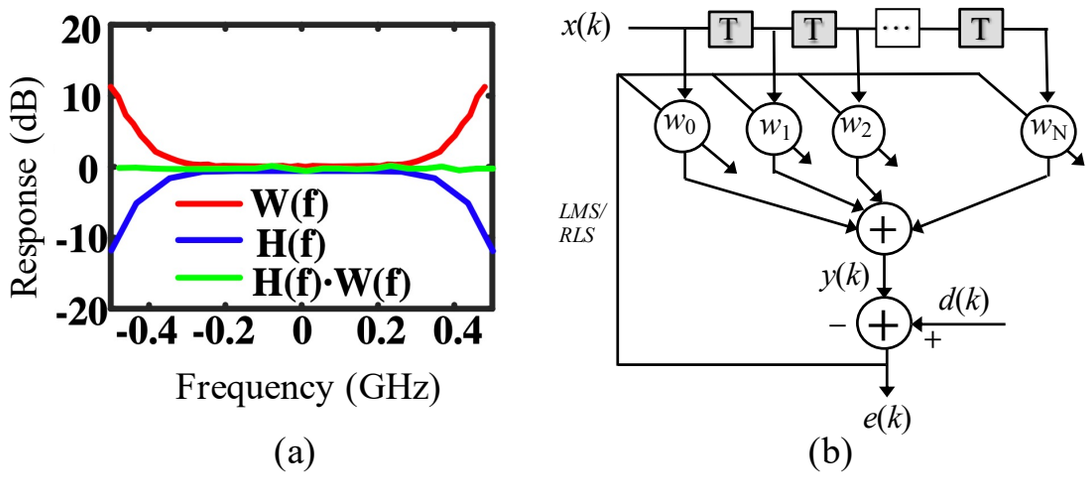

Figure 5.1: Equalization principle (a) and FFE equalizer (b).

in Fig. 5.1(b), whose input consists of the current and the delay symbols. After multiplying with the corresponding tap coefficients w_i, we can obtain the output expressed as

$$y(k) = \sum_{m=0}^{N} x[k-m]w_m. \tag{5.1}$$

Compared with the sending symbols, we can obtain the mean square error (MSE)

$$E\left(e^2(k)\right) = E\left[y^2(k) + d^2(k) + 2y(k)d(k)\right]. \tag{5.2}$$

The coefficients w_m can be updated by the least mean square (LMS) or recursive least squares (RLS) algorithm [155] until converging. From the structure point of view, the FFE is a finite impulse response (FIR) filter, which can only provide spectral zeros, and thus the FFE can effectively compensate when $H(f)$ is an all-pole response [156]. When there are spectral zeros in $H(f)$, the FFE not only fails to achieve effective compensation but also amplifies the in-band noise [156]. To avoid this effect, the decision feedback equalizer (DFE) is proposed with the structure shown in Fig. 5.2, which introduces spectral poles by adding a feedback structure after the FFE, so the spectral zeros and poles in $H(f)$ can be effectively compensated.

The error $e(k)$ can be expressed as

$$e(k) = \sum_{m=0}^{N} x[k-m]w_m - \sum_{j=0}^{L} d'[k-j]f_j \tag{5.3}$$

where $d'[k]$ is the decision output, w_m is the tapped coefficient of FFE, and f_j is the tapped coefficient of DFE. w_m and f_j are also obtained by using LMS to minimize the $E(e^2(k))$.

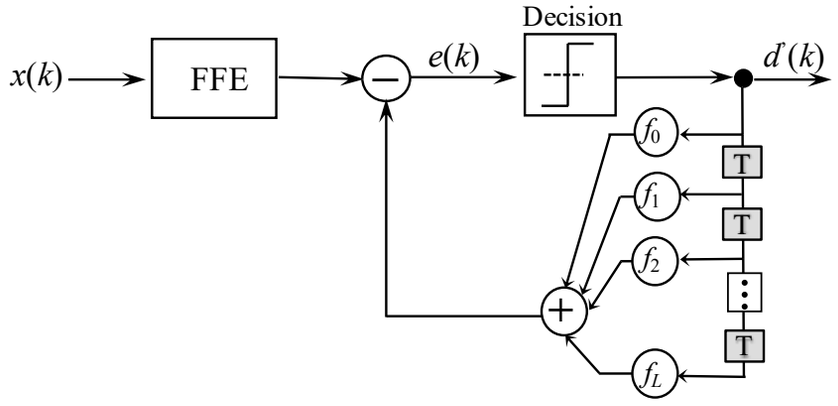

Figure 5.2: The structure of linear FFE-DFE.

5.1.2 Linear Tomlinson-Harashima precoding

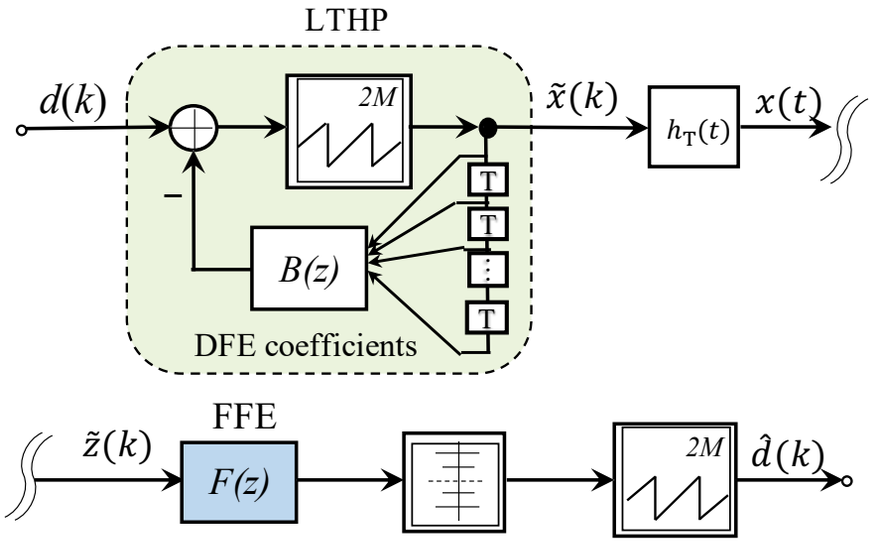

Figure 5.3: The structure of LTHP-FFE equalizer.

The feedback structure of the DFE takes into account the linear ISI caused by the decision symbols. However, when the output symbols are with the false decisions, this error may propagate because of the feedback structure, affecting the decision of the following symbols. To solve this problem, the feedback structure can be moved to the transmitter side so that the error propagation can be avoided. Based on this idea, the linear THP (LTHP)-FFE is proposed in [156]. The algorithm principle is presented in Fig. 5.3.

The LTHP-FFE needs to be processed at the transmitter and receiver sides separately, and its workflow is divided into three steps. For the first step, the FFE-DFE is used at the receiver side for the post-equalization. When the equalizer converges,

the feedback coefficients of DFE are retained as parameters of the LTHP. In the second step, the original symbols are pre-coded with LTHP at the transmitter side. To avoid instabilities induced by the feedback structure, the Modulo $2M$ operation is introduced to limit the transmit signal amplitude to the range of $-2M$ to $2M$. Here, M denotes the number of levels using the modulation code type, and for PAM-4, M is 4. The output signal after LTHP is expressed as

$$\tilde{x}(k) = d(k) - \sum_{i=0}^{N} \tilde{x}(k-i)w_i - 2Mb_k \tag{5.4}$$

where $d(k)$ is the sending symbols, and b_k is the integer that converts $\tilde{x}(k)$ to the range $(-2M, 2M)$. In the third step, the receiver uses FFE to equalize. Note that the target symbols of the FFE equalizer are no longer the original PAM-4 sequence $d(k)$, but the computed 8-level signal $x(k)$ during the training process, expressed as

$$x(k) = d(k) - 2Mb_k. \tag{5.5}$$

After the FFE equalization, $x(k)$ is then recovered to the original symbol $d'(k)$ by the Modulo $2M$ operation. Although LTHP-FFE can mitigate the error propagation of DFE, it is a linear superposition of symbols and thus can only compensate for linear impairment.

5.2 Nonlinear impairments compensation

5.2.1 Volterra filter

FFE, DFE, and THP-FFE consider only linear superposition of the input symbols. They cannot compensate for nonlinear impairments in the signal. To further mitigate the nonlinear impairments, the input symbols to the filter can be nonlinearly superimposed to introduce nonlinear features, like Volterra nonlinear equalizer and NN.

Fig. 5.4 shows a three-order Volterra filter. The output can be denoted by

$$\begin{aligned} y(n) = & \sum_{i_1=-k_1}^{k_1} w_{i_1} x\left(n+i_1\right) \\ & + \sum_{i_1=-k_2}^{k_2} \sum_{i_2=i_1}^{k_2} w_{i_1,i_2} x\left(n+i_1\right) x\left(n+i_2\right) \\ & + \sum_{i_1=-k_3}^{k_3} \sum_{i_2=i_1}^{k_3} \sum_{i_3=i_2}^{k_3} w_{i_1,i_2,i_3} x\left(n+i_1\right) x\left(n+i_2\right) x\left(n+i_3\right), \end{aligned} \tag{5.6}$$

where k_1, k_2, k_3 are the lengths of the first-, second-, and third-order kernels, respectively. (5.6) contains all the higher-order terms in the length range of each order. It introduces sufficient nonlinear features, so it has a strong nonlinear fitting ability and good equalization ability for communication channels with strong nonlinearities. However, as the length of the Volterra filter kernel increases, the number of filter taps increases sharply, and the computation complexity increases. Moreover, a large number of linear and nonlinear terms make little contribution to the equalization performance. Thus, the complexity of the Volterra filter can be simplified by pruning operations [153].

Volterra has a similar structure as FFE. Therefore, a decision feedback structure can be added to decrease the in-band noise. In **Paper D**, a joint NTHP-Volterra equalizer is proposed to further improve the performance of Volterra by combining the advantages of Volterra and THP, shown in Fig. 5.5.

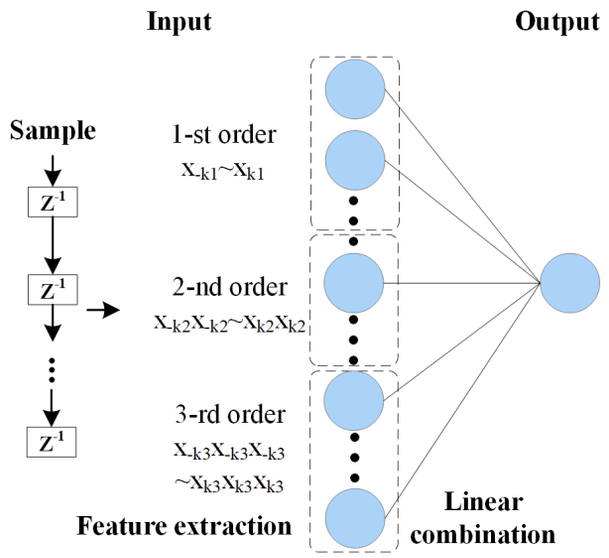

Figure 5.4: Structure of Volterra filter.

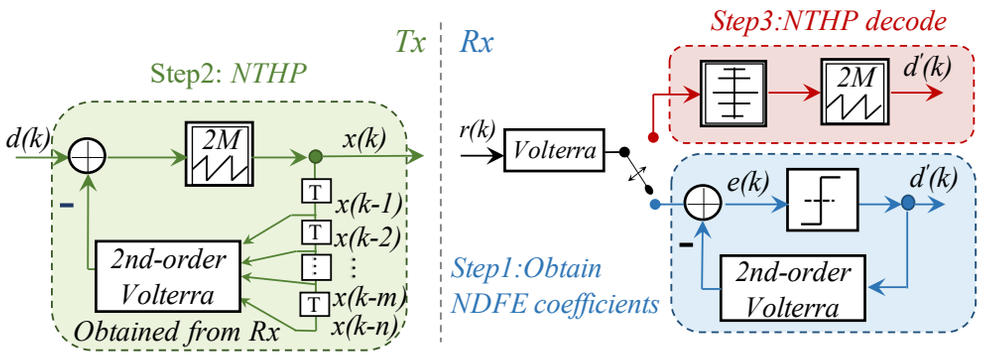

Figure 5.5: Block diagram of NTHP-Volterra equalizer.

The structure of NTHP-Volterra is similar to the LTHP-FFE except for replacing the linear FFE and DFE with the Volterra filter, addressing both linear and nonlinear impairments of the input and decision symbols. To show the effectiveness of NTHP-Volterra, the BER performance of 100G PAM-4 signal in an IMDD PON system with a 3 dB bandwidth of 15 GHz is evaluated. The BER result is shown in Fig. 5.6. Compared with the traditional FFE-DFE filter, LTHP-FFE can improve the receiver sensitivity by 1 dB since the error propagation is mitigated. Moreover, thanks to the nonlinearity compensation, 2 dB sensitivity improvement can be obtained by NTHP-Volterra compared with LTHP-FFE.

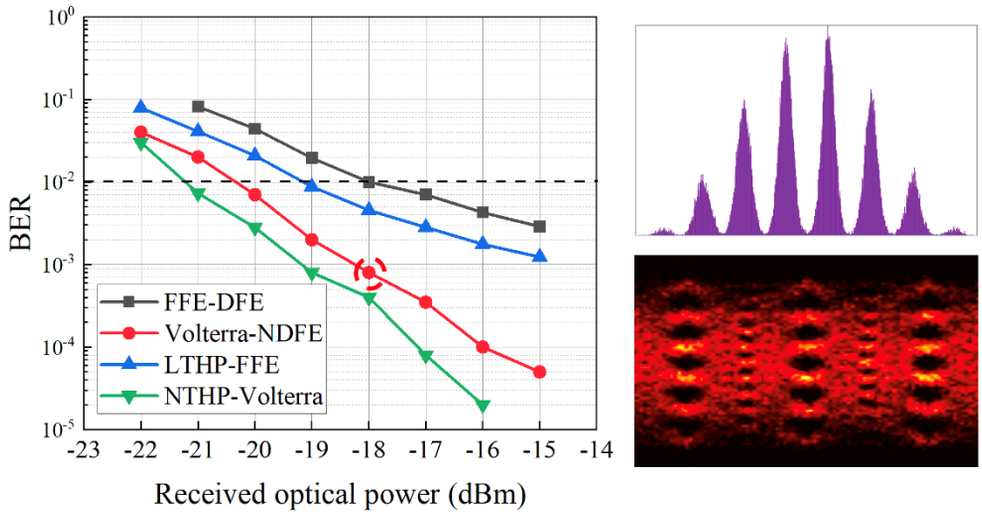

Figure 5.6: BER comparison of 100G PAM-4 signal with different equalizers after 20 km SMF.

5.2.2 Neural network

Compared with Volterra, NN has a more powerful nonlinear fitting capability. It has been proved that a NN consisting of two hidden layers can accurately represent arbitrary functions [157]. Accurate model estimation can be achieved by training the NN with the data sampled at the receiver side to compensate for linear and nonlinear distortions from the optical components and fibers during system transmission [158].

Fig. 5.7 shows a four-layer fully connected NN consisting of one input layer, two hidden layers, and one output layer, where the number of hidden layers can be adjusted according to the performance. For the input layer, the input signal is the same as FFE with the current and delayed symbols, while the hidden layer induces nonlinearity by using nonlinear activation function f. For each node at the hidden layer, its output can be expressed by

$$Y = f\left(\sum_{i=1}^{N} w_i x_i + b\right), \tag{5.7}$$

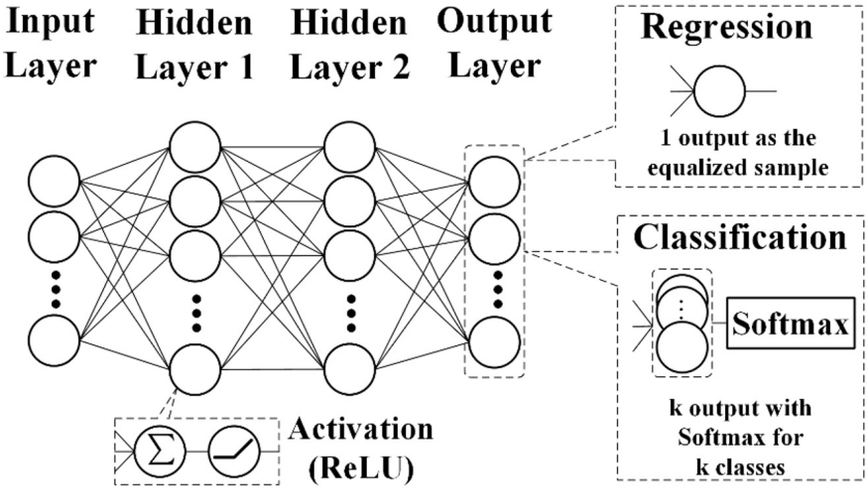

Figure 5.7: Architecture of neural network-based equalizer.

where $x = (x_0, x_1, \cdots, x_N)$ is the output value from nodes in the upper layer, and each of them has a coefficient w_i, and b is the bias. The commonly used nonlinear activation functions are Tanh, Sigmoid, Relu, etc., which satisfy the properties of continuous differentiable, nonlinear, and constant mapping [159].

In the output layer, the activation function is different from the hidden layer. When the purpose of NN is to complete the regression task, there is only one output node and no additional excitation functions. The linear weighting of the previous layer is the final output. If a classification task is preferred, the number of output nodes depends on the total number of categories. The activation function should be Softmax [160] which gives the probability of each category. Finally, gradient descent and back propagation are employed to minimize the loss function, i.e., MSE, and the coefficients are updated.

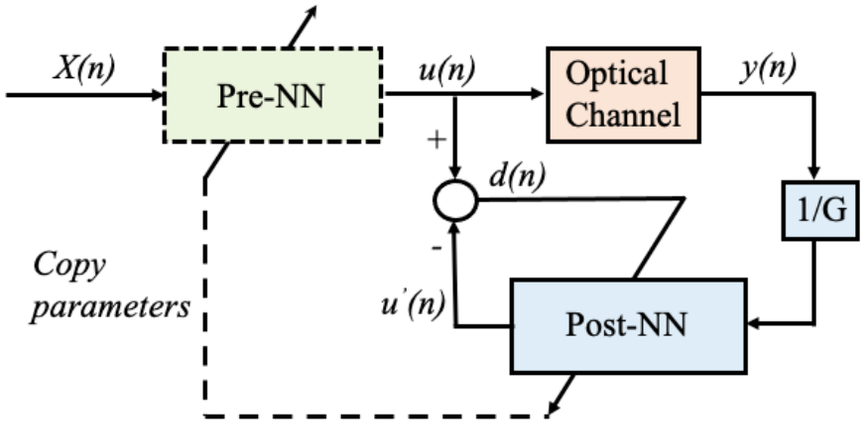

Figure 5.8: Architecture of NN based pre-equalizer.

However, NN's computational complexity is much higher than Volterra, which increases deployment costs if directly used at the ONU side. In **Paper E**, NN is

swapped to the OLT to compensate the SOA pattern effect for 50G PON so that the costs can be shared equally by multiple users and facilitate practical deployment. The architecture of the NN-based pre-equalizer is shown in Fig.5.8. To enable this swap, the NN at the receiving side needs to achieve accurate model estimation, ensuring the error $d(n)$ is close to 0. Also, the input signals of the pre- and post- NN need to be in the same power range, so the quantization factor G needs to be set reasonably.

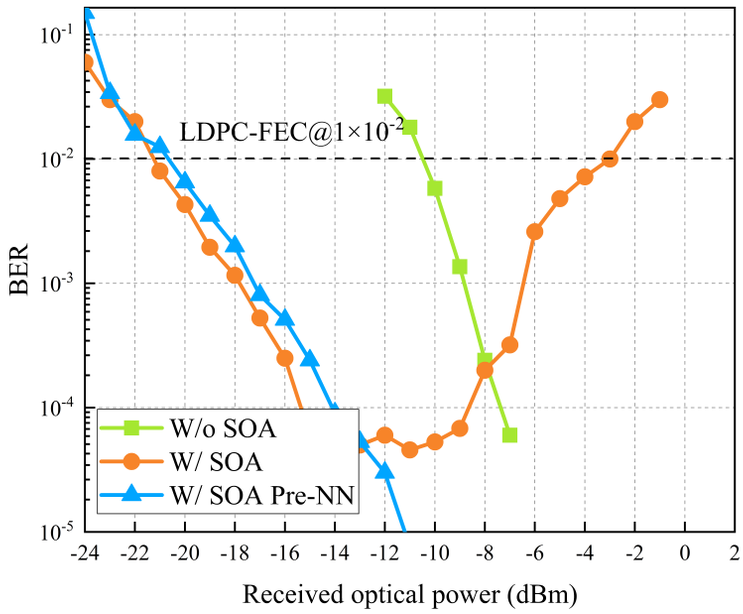

Figure 5.9: BER of 50 Gb/s PAM-4 signal with 20 km SMF at O-band with and without SOA.

As introduced in Chapter 3, the SOA pattern effect is a time-varying distortion. In order to obtain an accurate estimation of the SOA model, the post-NN is trained by doubled training data sampled at the two-time slots. In addition, the amplitude of the received signal should be normalized to -3 to 3 before being sent to the NN. When these two conditions are satisfied, the NN exchange from the ONU to the OLT works efficiently. The BER performance of 50 Gb/s PAM-4 signal with and without pre-NN is shown in Fig. 5.9. Without pre-NN, the BER starts to degrade when the received power exceeds -10 dBm, leading to a limited power receiving range. After employing pre-NN for pattern effect mitigation, the receiving dynamic range is significantly improved.

CHAPTER 6

Hybrid optical and digital signal processing

OSP and DSP schemes are introduced for impairments compensation in Chapter 4 and Chapter 5, respectively. This chapter introduces two hybrid optical and digital signal processing schemes for 50G PON with further performance improvement, compared with deploying DSP or OSP only. In **Paper F** and **Paper G**, DSE is employed at the OLT to pre-equalize the frequency response of bandwidth-limited directly modulated signal in the optical domain, so that the required DSP complexity in ONU is reduced. Similarly, in **Paper H**, by using injection locking in the transmitter side for bandwidth improvement and chirp compression, the transmission performance can be significantly improved combined with DSP at the receiver side.

6.1 Optics simplified DSP for 50G PAM-4 PON

In order to meet the performance requirement of 50G PON with low-cost 10G optics, complex DSP algorithms are required for impairments compensation, even in O-band [161]. Volterra can compensate for both linear and nonlinear distortions, but its complexity is too high for PON applications. Linear FFE and DFE with a simpler structure and lower complexity are preferable for 50G PON [162].

In **Paper F** and **G**, we experimentally illustrate 50G PAM-4 transmission using 10G optics. The experimental setup is shown in Fig. 6.1. A 10G O-band DML operating at 1310 nm is used for 50 Gb/s PAM-4 modulation. A spool of DSF with a dispersion of −150 ps/nm is followed for the DSE function. To compensate for

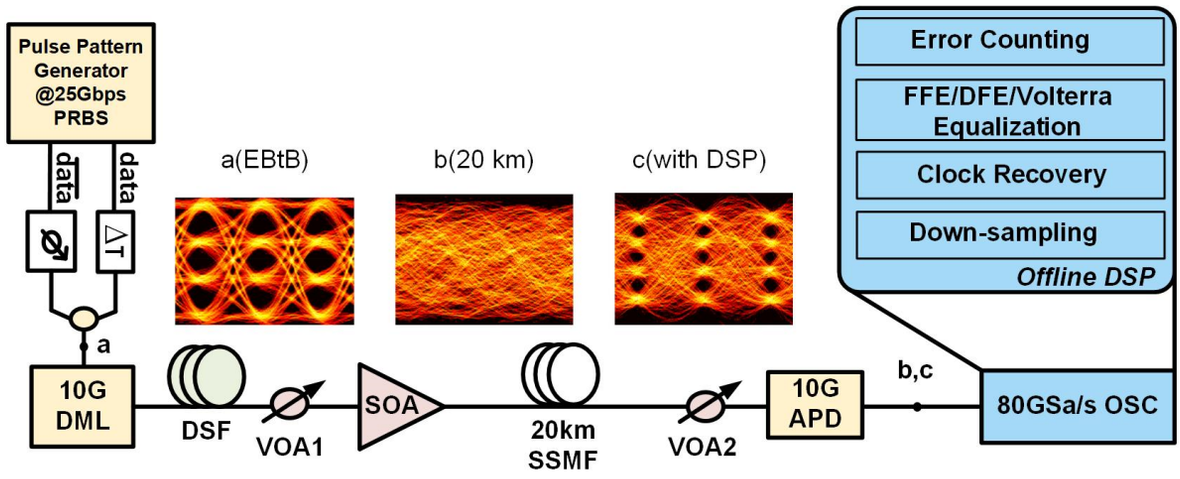

Figure 6.1: Experimental setup of 50G PON. Insets: (a) Electrical eye diagram at the input of the DML and eye diagrams after 20 km SMF transmission without (b) and with (c) DSP.

the insertion loss of DSF and also increase the launching power, an O-band SOA with a noise figure of 6.8 dB is used as a booster amplifier in the OLT. After fiber transmission, the signal is received by a 10G APD. Even with DSE, the eye diagram of 50 Gb/s PAM-4 signal is completely closed due to severe bandwidth limitation. Therefore, offline DSP is added for further compensation.

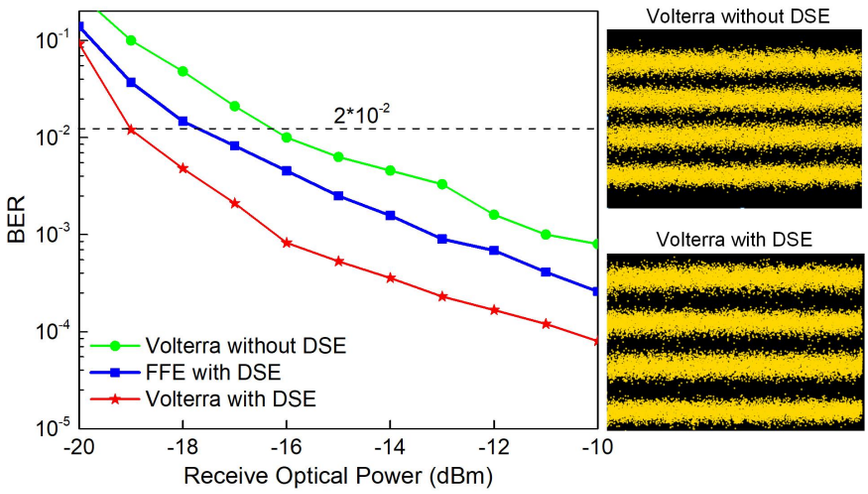

Figure 6.2: BER performances of 50-Gb/s PAM4 signal transmission over 20 km SMF for different equalization configurations.

Fig. 6.2 shows the BER performance of 50 Gb/s PAM4 signal transmission over 20 km SMF under three different equalization configurations in the O-band. Without DSE for pre-equalization, a three-order Volterra (30 15 5) filter can only achieve -16 dBm receiver sensitivity at the BER of 2×10^{-2}. After employing DSE, 3 dB sensitivity improvement can be obtained with the same Volterra, proving the

effectiveness of hybrid signal processing. In addition, with the help of DSE, 30-taps FFE filter is also able to achieve −18 dBm receiver sensitivity with 2 dB sensitivity improvement. For the three-order Volterra (30 15 5) filter, the required multiplier for each symbol is 185, while the 30-taps FFE filter only requires 30 multipliers [163]. Therefore, 2 dB sensitivity improvement are obtained after employing DSE, as well as reduced computation complexity is obtained.

6.2 50 Gb/s DMT transmission enabled by injection locking

For C-band 50G transmission with 10G DML, the signal quality is further degraded by DML chirp and CD. In Chapter 4, injection locking is introduced with the potential to compress the chirp and increase the bandwidth. In **Paper H**, we experimentally demonstrate 50 Gb/s DMT signal transmission over 20 km SMF with 10G DML in the C-band. The system configuration is illustrated in Fig. 6.3. The DMT signal is first generated in Matlab and then sent into a 50 GSa/s AWG. The output signal from the AWG is amplified to 1.5 Vpp and then loaded onto the 10G C-band DML, which is injection-locked by another DFB laser through an optical circulator. A polarization controller is used to match the polarization between two lasers. The spectra before and after injection locking is shown as inset. It can be observed that chirp-induced broaden spectra is compensated, leading to an improved dispersion tolerance of the system. After 20 km SMF transmission, the signal is detected by a 20G PD. Then the electrical signal is sampled and offline processed with DSP.

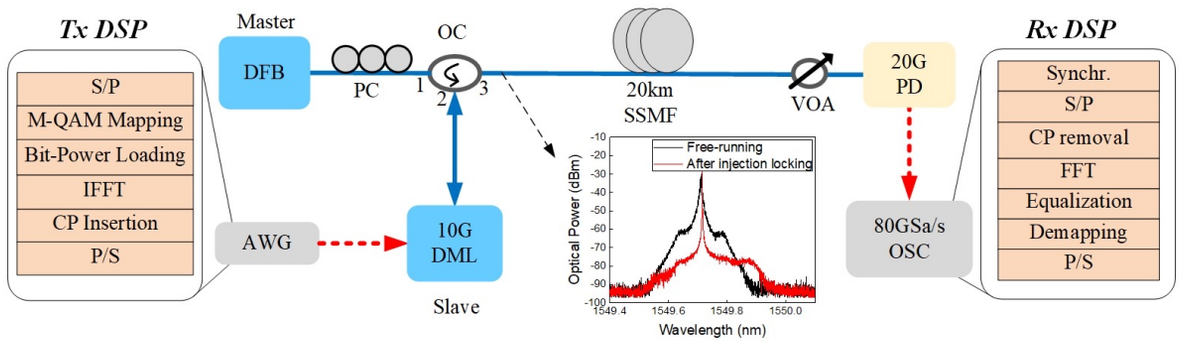

Figure 6.3: Experimental setup for 50G DMT transmission.

Fig. 6.4 shows SNR versus frequency with and without injection locking. It can be observed that the average SNR from different sub-carriers is improved from 11.62 dB to 15.61 dB after injection locking. The SNR dip due to the interaction between the fiber dispersion and DML chirp is moved from 5 GHz to 7 GHz due to the improved bandwidth. The BER performance is evaluated shown in Fig. 6.4(b). Without injection locking, only 25-Gb/s DMT transmission with free-running DML can be

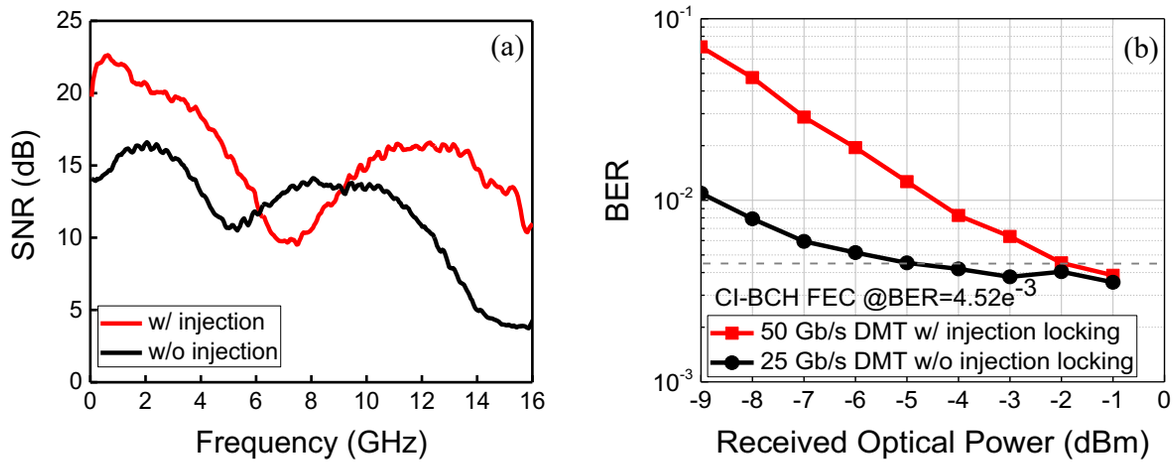

Figure 6.4: SNR versus frequency with and without injection locking (a) and BER versus received optical power after 20-km SMF transmission (b).

achieved at a BER of $4.52e^{-3}$ (BCH (CIBCH) FEC) [164]. After external injection, 50 Gb/s DMT signal transmission with a BER lower than the CI-BCH FEC limit is achieved, demonstrating that the system capacity can be doubled when optical injection locking is adopted.

CHAPTER 7

Future outlook

This thesis focuses on the key signal processing technologies in 25G, 50G, and 100G PONs. Some research progress has been made to provide some feasible and low-cost upgrade solutions for the next-generation PON standards. In this chapter, some interesting topics for further research are discussed.

Signal processing technologies in upstream

The work on single-wavelength 50G and 100G PONs in the paper mainly focus on the downlink direction, while there is less relevant research on the uplink direction. When the data rate in the uplink direct is upgraded to 100 Gb/s, DSP is also required. Since ONU and OLT have different cost sensitivity, the technology used in the uplink direction will also be different, so how to achieve uplink high-speed signal transmission needs further research.

Especially, unlike the downlink direction, the uplink user data is not sent in continuous mode, and there is a bursting mechanism. Burst mechanisms are sensitive to the system latency, and how to achieve fast equalization of high-speed uplink signals may need further research.

Machine learning in the PONs

Machine learning (ML) is a promising technology for nonlinearities compensation due to its powerful ability in nonlinear modeling. If the system with strong nonlinearities that are difficult to be described in mathematics, the ML methods often outperform traditional DSP algorithms in signal equalization. Recently, a group of

new ML methods like reinforcement learning, federated learning, and transfer learning are under comprehensive discussion in academia and industry. Their applications in PONs for specific transmission problems may need further investigation. Besides, most ML methods are based on supervised learning, which requires redundant data for training. Unsupervised ML can achieve full blind nonlinear equalization with only the received signal rather than original symbols, and it may also be beneficial for the un-cooling PONs with varying system status, e.g., wavelength shift. From another perspective, the computation complexity and the power consumption of machine learning algorithms are the biggest challenges for its application in the cost-sensitive PONs. Therefore, simplifying the computation complexity and speeding up the training process is also an interesting topic for the next step.

Low-cost coherent receiver design for future PONs

The demonstrations presented in this thesis are all based on low-cost IMDD technology. DSP and higher bandwidth optics are needed to address systems impairments and meet the power budget requirement. For the future of PONs (single-wavelength 200-400G PON), IMDD technology runs out of steam, and coherent technology seems the most logical technological choice. Coherent detection enables complex modulation in different dimensions, including phase, amplitude, and polarization. It also has the potential to provide a higher receiver sensitivity by simply increasing the local oscillator power. However, the traditional coherent receiver is costly, and the complex optics may add additional insertion losses to the system, leading to a degraded power budget. A Low-cost coherent receiver design will be a possible solution to improve the capacity and the power budget in future higher-speed PONs. Moreover, with the help of a coherent receiver, both the intensity and phase information can be recovered at the receiver side. Therefore, the signal processing technologies from the coherent optical communication field can be further investigated for their application in PONs.

CHAPTER 8

Summary of papers

In this chapter, a short summary of the publications included in this thesis is presented as well as the author's contribution.

Paper A

"First demonstration of symmetric 100G-PON in O-band with 10G-class optical devices enabled by dispersion-supported equalization," *Optical Fiber Communication Conference and Exhibition (OFC)*, paper M3H.1, Los Angeles, USA, 2017.

This paper presents an O-band demonstration of symmetric 100 Gb/s TWDM-PON with 10G optics. A spool of 10km dispersion-shifted fiber is employed to achieve multi-channel equalization in the optical domain. Symmetrical 4×25 Gb/s NRZ-OOK signal transmission can be achieved requiring no digital signal processing. A power budget of 26 dB downstream and 32 dB upstream are obtained.

My contribution: Original idea, built the experimental setup, conduct all measurements and analysis data, and wrote the manuscript.

Paper B

"Symmetric 100-Gb/s TWDM-PON based on 10G-class optical devices enabled by dispersion-supported equalization," *Journal of Lightwave Technology*, vol. 36, no. 2, pp. 580-586, 2018.

As an extension of Paper A, an SOA is added to compensate for the insertion loss of DSF and used as a pre-amplifier in upstream to increase the power budget. The influence of modulation voltage and drive current on the final equalization performance is also presented in detail.

My contribution: Original idea, built the experimental setup, conduct all measurements and analysis data, and wrote the manuscript.

Paper C

"First real-time demonstration of symmetric 100G-PON," *Asia Communications and Photonics Conference and Exhibition (ACP)*, paper AS4A.3, Wuhan, China, 2016.

This paper presents a C-band real-time demonstration of symmetric 100 Gb/s TWDM-PON using NRZ format based on 10G-class DML and photo-detectors. All optical and electrical components are integrated into a single OLT and an ONU line card. A multi-channel tunable dispersion compensator is employed for both downstream and upstream equalization. Finally, a power budget of 31 dB at BtB and 37 dB after 20 km fiber transmission are obtained.

My contribution: The OLT and ONU line board are fabricated by Fiber home. I built the experimental setup, perform all measurements and analysis data, and wrote the manuscript.

Paper D

"100G PAM-4 PON with 34 dB power budget using joint nonlinear Tomlinson-Harashima precoding and Volterra equalization," *European Conference and Exhibition on Optical Communication (ECOC)*, paper We4F.5, Bordeaux, France, 2021.

This paper presents a joint nonlinear equalization algorithm enabling single channel 100 Gb/s PAM-4 PON. The nonlinear THP and booster amplifier are employed in the OLT, and 34 dB power budget can be achieved.

My contribution: Original idea, built the experimental setup in IDLab imec-Ghent university, conduct all measurements and analysis data, and wrote the manuscript.

Paper E

"SOA pattern effect mitigation by neural network based pre-equalizer for 50G PON," *Optics Express*, vol. 16, no. 16, 2021.

In this paper, SOA pattern effect mitigation in a PAM-4 based 50G PON system is investigated. A neural network is employed to learn the nonlinear features of SOA by using two time-slots data for training. Moreover, the neural network is moved to OLT used as a pre-equalizer whose cost can be shared by all ONUs. Thanks to the pre-NN, the limited receiving dynamic range due to SOA pattern effect is significantly improved.

My contribution: Original idea, built the experimental setup, conduct all measurements and analysis data, and wrote the manuscript.

Paper F

"50-Gb/s TDM-PON based on 10g-class devices by optics-simplified DSP," *Optical Fiber Communication Conference and Exhibition (OFC)*, paper M2B.4, San Diego, USA, 2018.

This paper presents a demonstration of downstream 50 Gb/s PAM-4 PON with 10G DML and 10G APD. DSE is employed in the OLT to improve the signal quality partially in the optical domain, then only simple FFE in the ONU is needed. The DSE combined with FFE scheme shows 2 dB improvement than the complex Volterra algorithm, indicating its potential to reduce the complexity of DSP.

My contribution: Original idea, built the experimental setup, conduct all measurements and analysis data, and wrote the manuscript.

Paper G

"Optics-simplified DSP for 50 Gb/s PON downstream transmission using 10 Gb/s optical devices," *Journal of Lightwave Technology*, vol. 38, no. 3, pp. 583-589, 2020.

As an extension of Paper E, this paper adds the theoretical analysis and simulation of DSE performance in a 10G DML-based transmission system. The simulation result shows that the DSE can improve the 3-dB system bandwidth from 6 GHz to 11 GHz, which is consistent with the experiment result. On the other hand, a performance and computation complexity comparison among DSE+Volterra, DSE+FFE, and Volterra are presented. Finally, SOA is added to improve the system power budget.

My contribution: Original idea, built the experimental setup, conduct all measurements and analysis data, and wrote the manuscript.

Paper H

"50-Gb/s dispersion-unmanaged dmt transmission with injection locked 10G-class 1.55-µm DML," *Conference on Lasers and Electro-Optics (CLEO)*, paper SW4O.2, San Jose, USA, 2019.

In this paper, injection locking enabled C-band 50 Gb/s DMT transmission over 20 km SMF was presented. Thanks to the bandwidth improvement and chirp depression effect from injection locking, only 10G DML is required.

My contribution: Original idea, built the experimental setup, conduct all measurements and analysis data, and wrote the manuscript.

References

[1] Search Networking. (2017). "Definition of ARPANET," [Online]. Available: https://searchnetworking.techtarget.com/definition/ARPANET.

[2] V. Cisco, "Cisco visual networking index: Forecast and trends, 2017–2022," *White Paper*, 2018.

[3] N. S. Cisco, "Cisco annual internet report (2018–2023)," *White Paper*, 2020.

[4] J. Stanke. (2021). "Global broadband subscribers in Q1 2021," [Online]. Available: https://point-topic.com/free-analysis/global-broadband-subscribers-in-q1-2021.

[5] FTTH Council Europe, https://www.ftthcouncil.eu.

[6] Broadband Europe, https://ec.europa.eu/digital-single-market/en/broadband-europe.

[7] FTTH/B Market Panorama in europé. (2021), [Online]. Available: https://www.ftthcouncil.eu/knowledge-centre/all-publications-and-assets/191/european-ftth-b-market-panorama-2021.

[8] GlobeNewswire. (2020). "Global passive optical network equipment industry," [Online]. Available: https://www.globenewswire.com/news-release/2020/08/22/2082264/0/en/Global-Passive-Optical-Network-PON-Equipment-Industry.html.

[9] China Mobile Research Institute, "C-RAN: The road towards green ran," *White Paper*, 2013.

[10] P. Chanclou, A. Pizzinat, F. Le Clech, T.-L. Reedeker, Y. Lagadec, F. Saliou, B. Le Guyader, L. Guillo, Q. Deniel, S. Gosselin, *et al.*, "Optical fiber solution for mobile fronthaul to achieve C-RAN," *2013 Future Network and Mobile Summit (FuNeMS)*, Lisbon, Portugal, 2013.

[11] Y. Yifei and Z. Longming, "Application scenarios and enabling technologies of 5G," *China Communications*, vol. 11, no. 11, pp. 69–79, 2014.

[12] "Gigabit-capable passive optical networks (GPON): General characteristics," *ITU-T Recommendation G.984.1*, 2008, `https://www.itu.int/rec/T-REC-G.984.1-200803-I/en`.

[13] "40-Gigabit-capable passive optical network (NG PON2)," *ITU-T G.989.1*, 2013, `https://www.itu.int/rec/T-REC-G.989.1/e`.

[14] IEEE 802.3 Next Generation Ethernet Passive Optical Network (NG-EPON) Study Group, `https://ieee802.org/3/NGEPONSG/index.html`.

[15] "PON transmission technologies above 10 Gb/s per wavelength," *ITU-T Recommendation G.Sup64*, 2018, `https://www.itu.int/rec/T-REC-G.Sup64/en`.

[16] E. Harstead, "25G based PON technology," *Optical Fiber Communications Conference and Exposition (OFC)*, paper Tu2B.5, San Diego, USA, 2018.

[17] V. Houtsma and D. van Veen, "A study of options for high-speed TDM-PON beyond 10G," *Journal of Lightwave Technology*, vol. 35, no. 4, pp. 1059–1066, 2017.

[18] K. Zhang, H. He, H. Xin, W. Hu, S. Liang, D. Lu, and L. Zhao, "Chirp-aided power fading mitigation for upstream 100 km full-range long reach PON with DBR DML," *Optics Communications*, vol. 407, pp. 63–68, 2018.

[19] V. Houtsma and D. van Veen, "Demonstration of symmetrical 25 Gbps TDM-PON with 31.5 dB optical power budget using only 10 Gbps optical components," *Europe Conference on Optical Communication (ECOC)*, Valencia, Spain, 2015.

[20] R. Bonk, R. Borkowski, W. Pöhlmann, J. Van Kerrebrouck, C. Chase, R. Lucas, T. De Keulenaer, J. Bauwelinck, D. Van Veen, V. Houtsma, *et al.*, "Real-time demonstration of 28 Gbit/s electrical duobinary TDM-PON extension using remote nodes," *Optical Fiber Communications Conference and Exhibition (OFC)*, paper Th2A.27, Los Angeles, USA, 2017.

[21] V. E. Houtsma and D. T. van Veen, "Investigation of modulation schemes for flexible line-rate high-speed TDM-PON," *Journal of Lightwave Technology*, vol. 38, no. 12, pp. 3261–3267, 2020.

[22] J. K. Perin, M. Sharif, and J. M. Kahn, "Sensitivity improvement in 100 Gb/s-per-wavelength links using semiconductor optical amplifiers or avalanche photodiodes," *Journal of Lightwave Technology*, vol. 34, no. 23, pp. 5542–5553, 2016.

[23] R. Bonk, T. Vallaitis, J. Guetlein, C. Meuer, H. Schmeckebier, D. Bimberg, C. Koos, W. Freude, and J. Leuthold, "The input power dynamic range of a semiconductor optical amplifier and its relevance for access network applications," *Photonics Journal*, vol. 3, no. 6, pp. 1039–1053, 2011.

[24] L. A. Neto, J. Maes, P. Larsson-Edefors, J. Nakagawa, K. Onohara, and S. J. Trowbridge, "Considerations on the use of digital signal processing in future optical access networks," *Journal of Lightwave Technology*, vol. 38, no. 3, pp. 598–607, 2019.

[25] X. Tang, Y.-W. Chen, R. Zhang, S. Yao, Q. Zhou, S. Shen, M. Guo, Y. Qiao, and G.-K. Chang, "Low-complexity equalizer with a hybrid decision scheme for 50 Gb/s/λ PAM4-PON using a low-cost 10 G receiver," *Optics Letters*, vol. 45, no. 22, pp. 6278–6281, 2020.

[26] X. Tang, J. Zhou, M. Guo, J. Qi, T. Zhang, Z. Zhang, Y. Lu, and Y. Qiao, "An efficient nonlinear equalizer for 40-Gb/s PAM4-PON systems," *Optical Fiber Communications Conference and Exposition (OFC)*, paper W2A.62, San Diego, USA, 2018.

[27] M. Dalla Santa, "Next generation technologies for 100 Gb/s PON systems," Ph.D. dissertation, University College Cork, 2019.

[28] B. Skubic, E. I. de Betou, T. Ayhan, and S. Dahlfort, "Energy-efficient next-generation optical access networks," *IEEE Communications Magazine*, vol. 50, no. 1, pp. 122–127, 2012.

[29] K. Wang, C. M. Machuca, L. Wosinska, P. J. Urban, A. Gavler, K. Brunnstrom, and J. Chen, "Techno-economic analysis of active optical network migration toward next-generation optical access," *IEEE/OSA Journal of Optical Communications and Networking*, vol. 9, no. 4, pp. 327–341, 2017.

[30] A. Banerjee, Y. Park, F. Clarke, H. Song, S. Yang, G. Kramer, K. Kim, and B. Mukherjee, "Wavelength-division-multiplexed passive optical network (WDM-PON) technologies for broadband access: A review," *IEEE/OSA Journal of Optical Communications and Networking*, vol. 4, no. 11, pp. 737–758, 2005.

[31] B. Mukherjee, I. Tomkos, M. Tornatore, P. Winzer, and Y. Zhao, "Chaper 26.3.2: Beyond 10 Gb/s PONs," in *Handbook of Optical Networks*. Springer, 2020.

[32] G. Talli and P. D. Townsend, "Hybrid DWDM-TDM long-reach PON for next-generation optical access," *Journal of Lightwave Technology*, vol. 24, no. 7, pp. 2827–2834, 2006.

[33] J. D. Reis, A. Shahpari, R. Ferreira, S. Ziaie, D. M. Neves, M. Lima, and A. L. Teixeira, "Terabit+ (192×10 Gb/s) Nyquist shaped UDWDM coherent PON with upstream and downstream over a 12.8 nm band," *Journal of Lightwave Technology*, vol. 32, no. 4, pp. 729–735, 2013.

[34] F. El-Nahal and N. Hanik, "Technologies for future wavelength division multiplexing passive optical networks," *IET Optoelectronics*, vol. 14, no. 2, pp. 53–57, 2020.

[35] Y. Luo, X. Zhou, F. Effenberger, X. Yan, G. Peng, Y. Qian, and Y. Ma, "Time- and wavelength-division multiplexed passive optical network (TWDM-PON) for next-generation PON stage 2 (NG-PON2)," *Journal of Lightwave Technology*, vol. 31, no. 4, pp. 587–593, 2013.

[36] W. Shieh, H. Bao, and Y. Tang, "Coherent optical OFDM: Theory and design," *Optics Express*, vol. 16, no. 2, pp. 841–859, 2008.

[37] J. Armstrong, "OFDM for optical communications," *Journal of Lightwave Technology*, vol. 27, no. 3, pp. 189–204, 2009.

[38] K. Qiu, X. Yi, J. Zhang, H. Zhang, M. Deng, and C. Zhang, "OFDM-PON optical fiber access technologies," *Asia Communications and Photonics Conference and Exhibition (ACP)*, Shanghai, China, 2011.

[39] N. Cvijetic, "OFDM for next-generation optical access networks," *Journal of Lightwave Technology*, vol. 30, no. 4, pp. 384–398, 2011.

[40] "Full Service Access Network," `https://www.fsan.org/`.

[41] S. Gorshe, A. Raghavan, T. Starr, and S. Galli, *Broadband access: wireline and wireless-alternatives for internet services*. John Wiley & Sons, 2014.

[42] "ITU-T PON standards-progress and recent activities," 2018, `https://www.itu.int/en/ITU-T/studygroups/2017-2020/15/Documents/OFC2018-2-Q2_v5.pdf`.

[43] V. Houtsma, D. van Veen, and E. Harstead, "Recent progress on standardization of next-generation 25, 50, and 100G EPON," *Journal of Lightwave Technology*, vol. 35, no. 6, pp. 1228–1234, 2016.

[44] J. S. Wey, "The outlook for PON standardization: A tutorial," *Journal of Lightwave Technology*, vol. 38, no. 1, pp. 31–42, 2020.

[45] "Passive optical networks tutorial," `http://materias.fi.uba.ar/7543/download/PON_e1-jorge_finochietto.pdf`.

[46] "Broadband optical access systems based on passive optical networks (PON)," *ITU-T G.983.1*, `https://standards.globalspec.com/std/103304/ITU-TG.983.1`.

[47] "IEEE standard for information technology–local and metropolitan area networks–Part 3: CSMA/CD access method and physical layer specifications amendment: Media access control parameters, physical layers, and management parameters for subscriber access networks," *IEEE Std 802.3ah-2004*, pp. 1–640, 2004, `https://ieeexplore.ieee.org/document/1337489`.

[48] "Gigabit-capable passive optical networks (G-PON): Transmission convergence layer specification," *ITU-T G.984.3*, `https://www.itu.int/rec/T-REC-G.984.3`.

[49] "Physical layer specifications and management parameters for 10 Gb/s passive optical networks," *IEEE 802.3av*, https://ieeexplore.ieee.org/document/5294950.

[50] "10-Gigabit-capable passive optical networks (XG-PON): General requirements," *ITU-T G.987*, https://standards.globalspec.com/std/10046311/itu-t-g-987-1.

[51] "10-Gigabit-capable symmetric passive optical networks (XGS-PON) systems," *ITU-T G.9807*, https://www.itu.int/rec/T-REC-G.9807.1/en.

[52] "40-Gigabit-capable passive optical networks 2 (NG-PON2): Physical media dependent (PMD) layer specification," *ITU-T Recommendation G.989.2*, https://www.itu.int/rec/T-REC-G.989.2.

[53] "IEEE standard for ethernet, amendment 10: Media access control parameters, physical layers, and management parameters for 200Gb/s and 400Gb/s operation," *IEEE standard 802.3bs*, 2017, https://ieeexplore.ieee.org/document/8207825.

[54] "Physical layer specifications and management parameters for 25 Gb/s and 50 Gb/s passive optical networks," *IEEE P802.3ca*, https://www.ieee802.org/3/ca/.

[55] Y. Guo, Y. Yin, Y. Song, M. Huang, Y. Li, G. Kuang, Z. Fu, X. Huang, P. Cai, Z. Ma, *et al.*, "Demonstration of 25Gbit/s per channel NRZ transmission with 35 dB power budget using 25G Ge/Si APD for next generation 100G-PON," *Optical Fiber Communications Conference and Exhibition (OFC)*, paper M3H.6, Los Angeles, USA, 2017.

[56] M. Tao, J. Zheng, X. Dong, L. Zhou, H. Zeng, Y. Luo, S. Li, X. Liu, *et al.*, "Improved dispersion tolerance for 50G-PON downstream transmission via receiver-side equalization," *Optical Fiber Communications Conference and Exhibition (OFC)*, paper M2B.3, San Diego, USA, 2019.

[57] D. Nesset, "The progress of higher speed passive optical network standardization in ITU-T," *European Conference and Exhibition on Optical Communications (ECOC)*, paper We3F.1, Bordeaux, France, 2020.

[58] X. Yin, J. Lambrecht, G. Coudyzer, J. Verbist, H. Ramon, P. Ossieur, G. Torfs, and J. Bauwelinck, "Electronic circuits for high speed PON beyond 25G," *Optical Fiber Communications Conference and Exhibition (OFC)*, paper W4J.3, San Diego, USA, 2019.

[59] J. Wei, Q. Cheng, R. V. Penty, I. H. White, and D. G. Cunningham, "400 Gigabit ethernet using advanced modulation formats: Performance, complexity, and power dissipation," *IEEE Communications Magazine*, vol. 53, no. 2, pp. 182–189, 2015.

[60] ZTE, "Next generation fixed network access technologies," *White paper*, 2020.

[61] S. Walklin and J. Conradi, "Multilevel signaling for increasing the reach of 10 Gb/s lightwave systems," *Journal of Lightwave Technology*, vol. 17, no. 11, pp. 2235–2248, 1999.

[62] J. G. Proakis, *Digital communications*, fifth edition. Me Graw-Hill Education, 2007.

[63] T. Takahara, T. Tanaka, M. Nishihara, Y. Kai, L. Li, Z. Tao, and J. C. Rasmussen, "Discrete multi-tone for 100 Gb/s optical access networks," *Optical Fiber Communications Conference and Exhibition (OFC)*, paper p. M2I.1, San Francisco, USA, 2014.

[64] Y. Song, X. Yi, J. Zhang, X. Huang, Z. Zhang, and K. Qiu, "Comparison of dmt and PAM-4 in low-cost and bandwidth-limited optical fiber transmissions," *Asia Communications and Photonics Conference (ACP)*, paper S4B.1, Guangzhou, China, 2017.

[65] P. S. Chow, J. M. Cioffi, and J. A. Bingham, "A practical discrete multitone transceiver loading algorithm for data transmission over spectrally shaped channels," *IEEE Transactions on Communications*, vol. 43, no. 2/3/4, pp. 773–775, 1995.

[66] T. Starr, J. M. Cioffi, and P. J. Silverman, *Understanding digital subscriber line technology*. Englewood Cliffs, NJ: Prentice-Hall, 1999.

[67] D. Bykhovsky and S. Arnon, "An experimental comparison of different bit-and-power-allocation algorithms for DCO-OFDM," *Journal of Lightwave Technology*, vol. 32, no. 8, pp. 1559–1564, 2014.

[68] I. Geneva, "Discrete multitone technology for 100G ethernet (100GbE)," *Ethernet Technologies Summit*, 2012.

[69] R. Rath, D. Clausen, S. Ohlendorf, S. Pachnicke, and W. Rosenkranz, "Tomlinson–Harashima precoding for dispersion uncompensated PAM-4 transmission with direct-detection," *Journal of Lightwave Technology*, vol. 35, no. 18, pp. 3909–3917, 2017.

[70] D. van Veen and V. Houtsma, "Strategies for economical next-generation 50G and 100G passive optical networks," *Journal of Optical Communications and Networking*, vol. 12, no. 1, A95–A103, 2020.

[71] A. Lapidoth, *A Foundation in Digital Communication*. Cambridge University Press, 2009.

[72] Z. Li, M. S. Erkılınç, S. Pachnicke, H. Griesser, R. Bouziane, B. C. Thomsen, P. Bayvel, and R. I. Killey, "Signal-signal beat interference cancellation in spectrally-efficient WDM direct-detection Nyquist-pulse-shaped 16-QAM subcarrier modulation," *Optics Express*, vol. 23, no. 18, pp. 23 694–23 709, 2015.

[73] A. Oppenheim, W. A., and S. H. Naeab, *Signals and Systems*, 2nd Edition. Pearson, 1996.

[74] R. Nuyts, L. Tzeng, O. Mizuhara, and P. Gallion, "Effect of transmitter speed and receiver bandwidth on the eye margin performance of a 10-Gb/s optical fiber transmission system," *IEEE Photonics Technology Letters*, vol. 9, no. 4, pp. 532–534, 1997.

[75] D. T. van Veen and V. E. Houtsma, "Proposals for cost-effectively upgrading passive optical networks to a 25G line rate," *Journal of Lightwave Technology*, vol. 35, no. 6, pp. 1180–1187, 2017.

[76] Z. Zhou, M. Bi, S. Xiao, Y. Zhang, and W. Hu, "Experimental demonstration of symmetric 100-Gb/s DML-based TWDM-PON system," *IEEE Photonics Technology Letters*, vol. 27, no. 5, pp. 470–473, 2015.

[77] Z. Li, L. Yi, H. Ji, and W. Hu, "100-Gb/s TWDM-PON based on 10G optical devices," *Optics Express*, vol. 24, no. 12, pp. 12 941–12 948, 2016.

[78] V. Houtsma, D. van Veen, and E. Harstead, "Recent progress on standardization of next-generation 25, 50, and 100G EPON," *Journal of Lightwave Technology*, vol. 35, no. 6, pp. 1228–1234, 2016.

[79] H. Ji, L. Yi, Z. Li, L. Xue, X. Li, Q. Yang, S. Wang, Y. Yang, S. Yu, and W. Hu, "Field demonstration of a real-time 100-Gb/s PON based on 10G-class optical devices," *Journal of Lightwave Technology*, vol. 35, no. 10, pp. 1914–1921, 2017.

[80] J. Man, S. Fu, H. Zhang, J. Gao, L. Zeng, and X. Liu, "Downstream transmission of pre-distorted 25-Gb/s Faster-than-Nyquist PON with 10G-class optics achieving over 31 dB link budget without optical amplification," *Optical Fiber Communications Conference and Exhibition (OFC)*, paper Th1I.5, Anaheim, USA, 2016.

[81] D. van Veen, V. Houtsma, P. Winzer, and P. Vetter, "26-Gbps PON transmission over 40-km using duobinary detection with a low cost 7-GHz APD-based receiver," *European Conference and Exhibition on Optical Communications (ECOC)*, paper Tu.3.B.1, Amsterdam, Netherlands, 2012.

[82] J. Wei, K. Grobe, C. Sanchez, E. Giacoumidis, and H. Griesser, "Comparison of cost-and energy-efficient signal modulations for next generation passive optical networks," *Optics Express*, vol. 23, no. 22, pp. 28 271–28 281, 2015.

[83] X. Yin, J. Verbist, T. De Keulenaer, B. Moeneclaey, J. Verbrugghe, X.-Z. Qiu, and J. Bauwelinck, "25Gb/s 3-level burst-mode receiver for high serial rate TDM-PONs," *Optical Fiber Communication Conference*, paper Th4H.2, 2015.

[84] D. T. van Veen and V. E. Houtsma, "Symmetrical 25-Gb/s TDM-PON with 31.5-dB optical power budget using only off-the-shelf 10-Gb/s optical components," *Journal of Lightwave Technology*, vol. 34, no. 7, pp. 1636–1642, 2016.

[85] X. Li, S. Zhou, F. Gao, M. Luo, Q. Yang, Q. Mo, Y. Yu, and S. Fu, "4×28 Gb/s PAM4 long-reach PON using low complexity nonlinear compensation," *Optical Fiber Communication Conference*, paper M3H.4, Los Angeles, USA, 2017.

[86] C. Antony, M. Dalla Santa, G. Talli, and P. D. Townsend, "Raman amplification for O-band 25Gbps PAM-4 and duobinary using 10G optics," *European Conference on Optical Communication (ECOC)*, Gothenburg, Sweden, 2017.

[87] S. Barthomeuf, F. Saliou, L. A. Neto, B. Le Guyader, P. Chanclou, and D. Erasme, "Real-time downstream 25Gbit/s PAM4 for high speed TDM-PONs with both 25 and 12.5 Gbit/s ONUs," *Optical Fiber Communication Conference*, paper M1B.1, San Diego, USA, 2018.

[88] M. Tao, L. Zhou, H. Zeng, S. Li, and X. Liu, "50-Gb/s/λ TDM-PON based on 10G DML and 10G APD supporting PR10 link loss budget after 20-km downstream transmission in the O-band," *Optical Fiber Communications Conference and Exhibition (OFC)*, paper Tu3G.2, Los Angeles, USA, 2017.

[89] X. Miao, M. Bi, J. Yu, L. Li, and W. Hu, "SVM-modified-FFE enabled chirp management for 10G DML-based 50Gb/s/λ PAM4 IM-DD PON," *Optical Fiber Communication Conference*, paper M2B.5, San Diego, USA, 2019.

[90] N. Kaneda, D. van Veen, A. Mahadevan, and V. Houtsma, "DSP for 50G/100G hybrid modulated TDM-PON," *European Conference on Optical Communications (ECOC)*, Brussels, Belgium, 2020.

[91] J. Zhang, J. Yu, J. S. Wey, X. Li, L. Zhao, K. Wang, M. Kong, W. Zhou, J. Xiao, X. Xin, *et al.*, "SOA pre-amplified 100 Gb/s/λ PAM-4 TDM-PON downstream transmission using 10 Gbps O-band transmitters," *Journal of Lightwave Technology*, vol. 38, no. 2, pp. 185–193, 2020.

[92] N. H. Zhu, Z. Shi, Z. K. Zhang, Y. M. Zhang, C. W. Zou, Z. P. Zhao, Y. Liu, W. Li, and M. Li, "Directly modulated semiconductor lasers," *IEEE Journal of Selected Topics in Quantum Electronics*, vol. 24, no. 1, pp. 1–19, 2018.

[93] S. Matsuo and T. Kakitsuka, "Low-operating-energy directly modulated lasers for short-distance optical interconnects," *Advances in Optics and Photonics*, vol. 10, no. 3, pp. 567–643, 2018.

[94] V. E. Babicheva, A. Boltasseva, and A. V. Lavrinenko, "Transparent conducting oxides for electro-optical plasmonic modulators," *Nanophotonics*, vol. 4, no. 2, pp. 165–185, 2015.

[95] R. Amin, J. B. Khurgin, and V. J. Sorger, "Waveguide-based electro-absorption modulator performance: Comparative analysis," *Optics Express*, vol. 26, no. 12, pp. 15 445–15 470, 2018.

[96] Y. Fu, X. Zhang, B. Hraimel, T. Liu, and D. Shen, "Mach-zehnder: A review of bias control techniques for Mach-Zehnder modulators in photonic analog links," *IEEE Microwave Magazine*, vol. 14, no. 7, pp. 102–107, 2013.

[97] F. Koyama, "Recent advances of VCSEL photonics," *Journal of Lightwave Technology*, vol. 24, no. 12, pp. 4502–4513, 2006.

[98] J. A. Tatum, D. Gazula, L. A. Graham, J. K. Guenter, R. H. Johnson, J. King, C. Kocot, G. D. Landry, I. Lyubomirsky, A. N. MacInnes, *et al.*, "VCSEL-based interconnects for current and future data centers," *Journal of Lightwave Technology*, vol. 33, no. 4, pp. 727–732, 2015.

[99] Z. Xu, Y. J. Wen, W.-D. Zhong, C.-J. Chae, X.-F. Cheng, Y. Wang, C. Lu, and J. Shankar, "High-speed WDM-PON using CW injection-locked Fabry-Pérot laser diodes," *Optics Express*, vol. 15, no. 6, pp. 2953–2962, 2007.

[100] J. A. Lopera, A. M. Cárdenas, G. A. Quintero, J. D. Zapata, and J. J. G. Torres, "Low-reflective Fabry-Perot laser diode cavity as a colorless source on a WDM-PON system," *Photonic Networks and Devices*, paper NeTu2B.3, 2020.

[101] R. Gaudino, V. Curri, G. Bosco, G. Rizzelli, A. Nespola, D. Zeolla, S. Straullu, S. Capriata, and P. Solina, "On the use of DFB lasers for coherent PON," *Optical Fiber Communication Conference*, paper OTh4G.1, Los Angeles, USA, 2012.

[102] T. Horvath, P. Munster, and N.-H. Bao, "Lasers in passive optical networks and the activation process of an end unit: A tutorial," *Electronics*, vol. 9, no. 7, pp. 1–18, 2020.

[103] G. P. Agrawal and N. K. Dutta, *Long-wavelength semiconductor lasers*. New York, NY: Van Nostrand Reinhold Co. Inc., 1993.

[104] L.-S. Yan, Y. Wang, B. Zhang, C. Yu, J. McGeehan, L. Paraschis, and A. Willner, "Reach extension in 10-Gb/s directly modulated transmission systems using asymmetric and narrowband optical filtering," *Optics Express*, vol. 13, no. 13, pp. 5106–5115, 2005.

[105] Z. Li, L. Yi, W. Wei, M. Bi, H. He, S. Xiao, and W. Hu, "Symmetric 40-Gb/s, 100-km passive reach TWDM-PON with 53-dB loss budget," *Journal of Lightwave Technology*, vol. 32, no. 21, pp. 3391–3398, 2014.

[106] S. Zhou, X. Li, L. Yi, Q. Yang, and S. Fu, "Transmission of 2×56 Gb/s PAM-4 signal over 100 km SSMF using 18 GHz DMLs," *Optics Letters*, vol. 41, no. 8, pp. 1805–1808, 2016.

[107] Y. Matsui, D. Mahgerefteh, X. Zheng, C. Liao, Z. F. Fan, K. McCallion, and P. Tayebati, "Chirp-managed directly modulated laser (CML)," *IEEE Photonics Technology Letters*, vol. 18, no. 2, pp. 385–387, 2006.

[108] D. Che, F. Yuan, Q. Hu, and W. Shieh, "Frequency chirp supported complex modulation of directly modulated lasers," *Journal of Lightwave Technology*, vol. 34, no. 8, pp. 1831–1836, 2016.

[109] D. Che, F. Yuan, and W. Shieh, "Towards high-order modulation using complex modulation of semiconductor lasers," *Optics Express*, vol. 24, no. 6, pp. 6644–6649, 2016.

[110] C. Xie, P. Dong, P. Winzer, C. Gréus, M. Ortsiefer, C. Neumeyr, S. Spiga, M. Müller, and M.-C. Amann, "960-km SSMF transmission of 105.7-Gb/s PDM 3-PAM using directly modulated VCSELs and coherent detection," *Optics Express*, vol. 21, no. 9, pp. 11 585–11 589, 2013.

[111] P. Krehlik, "Directly modulated lasers in negative dispersion fiber links," *Opto-Electronics Review*, vol. 15, no. 2, pp. 71–77, 2007.

[112] E. Harstead, D. van Veen, V. Houtsma, and P. Dom, "Technology roadmap for time-division multiplexed passive optical networks (TDM PONs)," *Journal of Lightwave Technology*, vol. 37, no. 2, pp. 657–664, 2019.

[113] R. Koma, M. Fujiwara, J.-i. Kani, S.-Y. Kim, T. Suzuki, K.-I. Suzuki, and A. Otaka, "Demonstration of real-time burst-mode digital coherent reception with wide dynamic range in DSP-based PON upstream," *Journal of Lightwave Technology*, vol. 35, no. 8, pp. 1392–1398, 2017.

[114] G. P. Agrawal and N. A. Olsson, "Self-phase modulation and spectral broadening of optical pulses in semiconductor laser amplifiers," *IEEE Journal of Quantum Electronics*, vol. 25, no. 11, pp. 2297–2306, 1989.

[115] L. Xue, L. Yi, R. Lin, L. Huang, and J. Chen, "SOA pattern effect mitigation by neural network based pre-equalizer for 50G PON," *Optics Express*, vol. 29, no. 16, pp. 24 714–24 722, 2021.

[116] S. Aleksic and V. Krajinovic, "Methods for compensation of the pattern effect in semiconductor optical amplifiers," *European Conference on Networks and Optical Communications (ECOC)*, 2003.

[117] K. Inoue, "Optical filtering technique to suppress waveform distortion induced in a gain-saturated semiconductor optical amplifier," *Electronics Letters*, vol. 33, no. 10, pp. 885–886, 1997.

[118] A. Ghazisaeidi and L. A. Rusch, "On the efficiency of digital back-propagation for mitigating SOA-induced nonlinear impairments," *Journal of Lightwave Technology*, vol. 29, no. 21, pp. 3331–3339, 2011.

[119] K. Wang, J. Zhang, L. Zhao, X. Li, and J. Yu, "Mitigation of pattern-dependent effect in SOA at O-band by using DSP," *Journal of Lightwave Technology*, vol. 38, no. 3, pp. 590–597, 2020.

[120] G. P. Agrawal, *Fiber-optic communication systems*. John Wiley & Sons, 2002.

[121] Cisco, "Fiber types in gigabit optical communications," Technical Report, 2008.

[122] H. Ji, L. Yi, L. Xue, and W. Hu, "Upstream dispersion management of 25 Gb/s duobinary and PAM-4 signals to support 0–40 km differential reach," *Chinese Optics Letters*, vol. 15, no. 2, pp. 0 225 021–0 225 025, 2017.

[123] M. Kaur and H. Sarangal, "Analysis on dispersion compensation with dispersion compensation fiber (DCF)," *SSRG International Journal of Electronics and Communication Engineering (SSRG-IJECE)*, 2015.

[124] E. Agrell, M. Karlsson, A. Chraplyvy, D. J. Richardson, P. M. Krummrich, P. Winzer, K. Roberts, J. K. Fischer, S. J. Savory, B. J. Eggleton, *et al.*, "Roadmap of optical communications," *Journal of Optics*, vol. 18, no. 6, p. 063 002, 2016.

[125] P. J. Winzer, D. T. Neilson, and A. R. Chraplyvy, "Fiber-optic transmission and networking: The previous 20 and the next 20 years," *Optics Express*, vol. 26, no. 18, pp. 24 190–24 239, 2018.

[126] Z. Zhang, Q. Guo, C. Ju, S. Cai, L. Wang, M. Zhang, and X. Chen, "Optical- and electrical-domain compensation techniques for next-generation passive optical networks," *IEEE Communications Magazine*, vol. 57, no. 4, pp. 144–150, 2019.

[127] K. Iwashita and N. Takachio, "Chromatic dispersion compensation in coherent optical communications," *Journal of Lightwave Technology*, vol. 8, no. 3, pp. 367–375, 1990.

[128] T. Xu, G. Jacobsen, S. Popov, J. Li, E. Vanin, K. Wang, A. T. Friberg, and Y. Zhang, "Chromatic dispersion compensation in coherent transmission system using digital filters," *Optics Express*, vol. 18, no. 15, pp. 16 243–16 257, 2010.

[129] A. Mecozzi, C. Antonelli, and M. Shtaif, "Kramers–Kronig coherent receiver," *Optica*, vol. 3, no. 11, pp. 1220–1227, 2016.

[130] H. Kogelnik, R. M. Jopson, and L. E. Nelson, "Polarization-mode dispersion," in *Optical Fiber Telecommunications IV-B*, 2002, pp. 725–861.

[131] B.-n. Hu, W. Jing, W. Wei, and R.-m. Zhao, "Analysis on dispersion compensation with DCF based on optisystem," *International Conference on Industrial and Information Systems*, paper pp. 40–43, 2010.

[132] A. B. Dar and R. K. Jha, "Chromatic dispersion compensation techniques and characterization of fiber bragg grating for dispersion compensation," *Journal of Optical and Quantum Electronics*, vol. 49, no. 108, pp. 1–35, 2017.

[133] C. Yang, R. Hu, M. Luo, Q. Yang, C. Li, H. Li, and S. Yu, "IM/DD-based 112-Gb/s/λ PAM-4 transmission using 18-Gbps DML," *IEEE Photonics Journal*, vol. 8, no. 3, pp. 1–7, 2016.

[134] M. Tanaka and M. Shigematsu, "10Gbit/s directly modulated signal transmission over 80km SMF with chirp compensation using four-wave mixing," *Conference on Lasers and Electro-Optics/International Quantum Electronics Conference and Photonic Applications Systems Technologies*, paper CThG1, 2004.

[135] W. Wei, L. Yi, Y. Jaouën, M. Morvan, and W. Hu, "Brillouin rectangular optical filter with improved selectivity and noise performance," *IEEE Photonics Technology Letters*, vol. 27, no. 15, pp. 1593–1596, 2015.

[136] J. Wang and K. Petermann, "Small signal analysis for dispersive optical fiber communication systems," *Journal of Lightwave Technology*, vol. 10, no. 1, pp. 96–100, 1992.

[137] K. Y. Lau and A. Yariv, "Ultra-high speed semiconductor lasers," *IEEE Journal of Quantum Electronics*, vol. QE-21, pp. 121–137, 1985.

[138] R. Lang, "Injection locking properties of a semiconductor laser," *IEEE Journal of Quantum Electronics*, vol. 18, no. 6, pp. 976–983, 1982.

[139] J. Wang, M. Haldar, L. Li, and F. Mendis, "Enhancement of modulation bandwidth of laser diodes by injection locking," *IEEE Photonics Technology Letters*, vol. 8, no. 1, pp. 34–36, 1996.

[140] A. Moscoso-Mártir, J. Müller, J. Hauck, N. Chimot, R. Setter, A. Badihi, D. E. Rasmussen, A. Garreau, M. Nielsen, E. Islamova, *et al.*, "Silicon photonics transmitter with SOA and semiconductor mode-locked laser," *Scientific Reports*, vol. 7, no. 1, pp. 13857/1–13, 2017.

[141] E. K. Lau, X. Zhao, H.-K. Sung, D. Parekh, C. Chang-Hasnain, and M. C. Wu, "Strong optical injection-locked semiconductor lasers demonstrating $>$ 100-GHz resonance frequencies and 80-GHz intrinsic bandwidths," *Optics Express*, vol. 16, no. 9, pp. 6609–6618, 2008.

[142] S. Mohrdiek, H. Burkhard, and H. Walter, "Chirp reduction of directly modulated semiconductor lasers at 10 Gb/s by strong CW light injection," *Journal of Lightwave Technology*, vol. 12, no. 3, pp. 418–424, 1994.

[143] X. Zhao, B. Zhang, L. Christen, D. Parekh, W. Hofmann, M. C. Amann, F. Koyama, A. E. Willner, and C. J. Chang-Hasnain, "Greatly increased fiber transmission distance with an optically injection-locked vertical-cavity surface-emitting laser," *Optics Express*, vol. 17, no. 16, pp. 13 785–13 791, 2009.

[144] M. T. A. Khan, E. Alkhazraji, A. M. Ragheb, H. Fathallah, K. Qureshi, S. Alshebeili, and M. Khan, "100 Gb/s single channel transmission using injection-locked 1621 nm quantum-dash laser," *IEEE Photonics Technology Letters*, vol. 29, no. 6, pp. 543–546, 2017.

[145] M.-C. Cheng, C.-T. Tsai, Y.-C. Chi, and G.-R. Lin, "Direct QAM-OFDM encoding of an L-band master-to-slave injection-locked WRC-FPLD pair for 28×20 Gb/s DWDM-PON transmission," *Journal of Lightwave Technology*, vol. 32, no. 17, pp. 2981–2988, 2014.

[146] K. Panajotov, Q. T. Nguyen, M. Sciamanna, P. Besnard, L. Bramerie, A. A. Valle, R. Michalzik, A. Shen, A. Garreau, O. Vaudel, C. Kazmierski, G.-H. Duan, and J.-C. Simon, "Using optical injection of Fabry-Perot lasers for high-speed access in optical telecommunications," *Progress in Electromagnetic Research Symposium (PIERS)*, Brussel, Belgium, 2012.

[147] H.-K. Sung, E. K. Lau, and M. C. Wu, "Optical single sideband modulation using strong optical injection-locked semiconductor lasers," *IEEE Photonics Technology Letters*, vol. 19, no. 13, pp. 1005–1007, 2007.

[148] B. Schrenk, M. Hofer, and T. Zemen, "Analog receiver for coherent optical analog radio-over-fiber transmission," *Optics Letters*, vol. 42, no. 16, pp. 3165–3168, 2017.

[149] J. Tao, P. Wang, L. Huang, Y. Zhang, D. Chen, P. Xiang, J. Zheng, G.-W. Lu, X. Chen, and T. Pu, "All-optical signal upconversion using optically-injected DFB laser and embedded optoelectronic oscillator for radio-over-fiber applications," *Optical Fiber Communications Conference and Exhibition (OFC)*, paper Tu2F.2, Los Angeles, USA, 2017.

[150] N. Kaneda, R. Zhang, Y. Lefevre, A. Mahadevan, D. van Veen, and V. Houtsma, "First experimental demonstration of flexible rate PON beyond 100Gb/s with probabilistic and geometric shaping," *Optical Fiber Communication Conference*, paper F2H.2, 2021.

[151] Y. Fu, D. Kong, H. Xin, M. Bi, S. Jia, K. Zhang, W. Hu, and H. Hu, "Computationally efficient 120 Gb/s/λ PWL equalized 2D-TCM-PAM8 in dispersion unmanaged DML-DD system," *Optical Fiber Communication Conference (OFC)*, paper T3I.5, San Diego, USA, 2020.

[152] X. Tang, J. Zhou, M. Guo, J. Qi, F. Hu, Y. Qiao, and Y. Lu, "40-Gb/s PAM4 with low-complexity equalizers for next-generation PON systems," *Optical Fiber Technology*, vol. 40, pp. 108–113, 2018.

[153] L. Tao, H. Tan, C. Fang, and N. Chi, "Simplified volterra series based nonlinear equalization in short reach optical transmissions," *Progress in Electromagnetic Research Symposium (PIERS)*, Shanghai, China, 2016.

[154] D. Li, H. Song, W. Cheng, M. Cheng, S. Fu, M. Tang, D. Liu, and L. Deng, "Low-complexity equalization scheme for suppressing FFE-enhanced in-band noise and ISI in 100 Gbps PAM4 optical IMDD system," *Optics Letters*, vol. 45, no. 9, pp. 2555–2558, 2020.

[155] P. S. R. Diniz, *Adaptive Filtering: Algorithms and Practical Implementation*. Springer, 2014.

[156] R. F. H. Fischer, *Precoding and Signal Shaping for Digital Transmission*. John Wiley & Sons, 2002.

[157] M. Nielsen. (2019). "Neural networks and deep learning," [Online]. Available: `http://neuralnetworksanddeeplearning.com`.

[158] K. Burse, R. N. Yadav, and S. Shrivastava, "Channel equalization using neural networks: A review," *IEEE Transactions on Systems, Man, and Cybernetics*, vol. 40, no. 3, pp. 352–357, 2010.

[159] I. Goodfellow, Y. Bengio, and A. Courville, *Deep learning*. The MIT press, 2018.

[160] L. Yi, T. Liao, L. Huang, L. Xue, P. Li, and W. Hu, "Machine learning for 100 Gb/s/λ passive optical network," *Journal of Lightwave Technology*, vol. 37, no. 6, pp. 1621–1630, 2019.

[161] D. Zhang, D. Liu, X. Wu, and D. Nesset, "Progress of ITU-T higher speed passive optical network (50G-PON) standardization," *Journal of Optical Communications and Networking*, vol. 12, no. 10, pp. D99–D108, 2020.

[162] B. Li, K. Zhang, D. Zhang, J. He, X. Dong, Q. Liu, and S. Li, "Dsp enabled next generation 50G TDM-PON," *Journal of Optical Communications and Networking*, vol. 12, no. 9, pp. D1–D8, 2020.

[163] K. Zhong, X. Zhou, T. Gui, L. Tao, Y. Gao, W. Chen, J. Man, L. Zeng, A. P. T. Lau, and C. Lu, "Experimental study of PAM-4, CAP-16, and DMT for 100 Gb/s short reach optical transmission systems," *Optics Express*, vol. 23, no. 2, pp. 1176–1189, 2015.

[164] M. Scholten, T. Coe, and J. Dillard, "Continuously- interleaved BCH (CIBCH) FEC delivers best in class NECG for 40G and 100G metro applications," *Optical Fiber Communication Conference and Exhibition (OFC)*, paper NTuB3, San Diego, USA, 2010.